Title
The Sensorimotor Basis of Predator Evasion for Larval Zebrafish

Permalink
https://escholarship.org/uc/item/4s19b2zm

Author
Nair, Arjun Madan

Publication Date
2017

Peer reviewed|Thesis/dissertation

UNIVERSITY OF CALIFORNIA,
IRVINE

The Sensorimotor Basis of Predator Evasion for Larval Zebrafish

DISSERTATION

submitted in partial satisfaction of the requirements
for the degree of

DOCTOR OF PHILOSOPHY

in Biological Sciences

by

Arjun Madan Nair

Dissertation Committee:
Professor Matthew James McHenry, Chair
Professor Timothy J. Bradley
Assistant Professor Emanuel Azizi

2017

DEDICATION

To

My loving family,
My supportive friends,
And my dear partner in life, Simei Yeh

TABLE OF CONTENTS

LIST OF FIGURES

LIST OF TABLES

ACKNOWLEDGMENTS

CURRICULUM VITAE

Arjun Madan Nair

EDUCATION

2017   Ph.D. in Biological Sciences, with a concentration in Ecology and Evolutionary Biology, University of California, Irvine.
Dissertation title: The sensorimotor basis of predator evasion for larval zebrafish

2015   M.S. in Biological Sciences, with a concentration in Ecology and Evolutionary Biology, University of California, Irvine.

2011   B.S. in Biomedical Engineering
University of California, Davis.
Emphasis: Systems engineering with a computational background

APPOINTMENTS

2016   Adjunct Instructor, Department of Biology
Santa Ana College

2015-16   California Community College Intern
Santa Ana College

2015   Instructor, Department of Ecology and Evolutionary Biology
University of California, Irvine

2012-16   Teaching Assistant, Department of Ecology and Evolutionary Biology
University of California, Irvine

2011-12   System Biology Graduate Fellow, Center of Complex Biological System
University of California, Irvine

PUBLICATIONS

Nair, A., Azatian, G. and McHenry, M. (2015). The kinematics of directional control in the fast start of zebrafish larvae. *Journal of Experimental Biology* 218, 3996-4004.

Stewart, W., Nair, A., Jiang, H. and McHenry, M. (2014). Prey fish escape by sensing the bow wave of a predator. *Journal of Experimental Biology* 217, 4328-4336.

Yao, A., Fenton, T., Owsley, K., Seitzer, P., Larsen, D., Sit, H., Lau, J., Nair, A., Tantiongloc, J., Tagkopoulos, I. and Facciotti, M (2013). Promoter Element Arising from the Fusion of Standard BioBrick Parts. *ACS Synthetic Biology* 2, 111–120.

Skommer, J., Das, S., Nair, A., Brittain, T. and Raychaudhuri, S. (2011). Nonlinear regulation of commitment to apoptosis by simultaneous inhibition of Bcl-2 and XIAP in leukemia and lymphoma cells. *Apoptosis* 6, 619-26.

AWARDS AND FELLOWSHIPS

2016   Grover C. Stephen Fellowship for Comparative Physiology
     University of California, Irvine

2013   Best Student Poster Presentation, Division of Biomechanics
     SICB Annual meeting, San Francisco, CA

2011-12 Mathematical, Computational Biology Fellowship
     University of California, Irvine

ABSTRACT OF THE DISSERTATION

The sensorimotor basis of predator evasion for larval zebrafish

By

Arjun Madan Nair

Doctor of Philosophy in Biological Sciences,

With a concentration in Ecology and Evolutionary Biology

University of California, Irvine, 2017

Professor Matthew James McHenry, Chair

Predator-prey interactions are critical to the biology of fishes, but it is unclear how sensory and motor systems of prey fish impact predator evasion. In this dissertation, I present work that provides a better understanding of how a prey's sensorimotor system can impact its survival of a predatory encounter. The results of my dissertation give a holistic view of how physiology, behavior and game theory can be used to explain predator evasion in larval zebrafish.

My first dissertation chapter described how larval zebrafish use a fast start to move with three-dimensional trajectories. Classically, fast starts have been described purely as a two-dimensional motion. However, in previous studies anecdotal evidence suggested that larval zebrafish can escape in three dimensions. To study this phenomenon, I made careful three-dimensional kinematic measures of larval zebrafish performing fast starts. The first dissertation chapter revealed that rotations of the larvae's body around its center of mass were indicative of the three-dimensional trajectory the whole body translated towards.

My second dissertation chapter investigated the relative importance between the sensory and motor systems in prey survival in a predator-prey interaction. Many studies have studied the

importance of the sensory and motor system for predator evasion, but no study has measured one system's importance to survival relative to the other system. In the second chapter, I created a probabilistic, agent-based model to simulate predator-prey interactions between adult and larval zebrafish *in silico*. After running the model with varying parameter changes, I observed that the sensory system of a larval zebrafish had a greater impact on prey survival than its motor system.

My third chapter studied the escape strategy of larval zebrafish. Prey fish have an algorithm to choose an escape direction to flee with. However, there are two competing school of thought about how prey fish should choose their escape direction. In my third chapter, I recorded larval zebrafish reactions to a robotic predator and measure escape angles. My investigations revealed that larval zebrafish use a mixed strategy that combined both competing theories of escape strategy.

INTRODUCTION

Predator-prey interactions have significant effects on population dynamics, biodiversity and the ecosystem (Barbosa and Castellanos 2005, Terborgh and Estes 2010, Curios 2012). Although the effects of predation are studied on the population scale, the act of predation itself works on the individual scale as predator-prey interactions, where one predator attempts to engage and capture its prey. Despite the copious amounts of knowledge on predation on the macroscopic scale, piscivorous predator-prey interactions are still not well understood, despite its obvious value in commercial industries, such as fisheries. Therefore, a goal of this dissertation is to broaden our comprehension of piscivorous predator-prey interactions, particularly by developing a framework to understand how prey fish survive predatory events with larger predator fish.

For prey fish to survive predation, the prey's sensory and motor capabilities are extremely vital. Understanding the sensorimotor basis of escape is imperative for understanding prey fish survival (Dill 1974, Korn and Faber 2008). The sensory and motor faculties of a prey fish are important for various aspects of piscivorous predator-prey interactions. For instance, in a piscivorous predator-prey interaction, the predator fish approaches its prey head on in attempt to capture the prey. When the predator approaches its prey, the prey fish must be able to detect the oncoming threat by using its sensory systems. Once a threat is detected, prey fish must engage their motor system to evade the predator by committing to an escape response, propelling the prey away from the predator. After moving away from the threat, the prey fish must repeat the cycle by searching their surrounding again to see if the predator continues its pursuit, consequently escaping again if necessary. Escaping an approaching predator is a rapid behavioral

1

response that involves an intricate interplay between the fish's sensory and motor system. Failure to execute this sensorimotor loop will result in the prey's capture and quick demise.

In general, the sensorimotor basis of predator evasion in piscivorous predator-prey interactions is not well studied. In recent years, there have been efforts to understand how fish use their sensory and motor system to evade predatory strikes (O'Malley et al. 1996, McHenry and Liao 2011, Stewart et al. 2014, Dunn et al. 2016). Also, there has also been a growing body of literature about how the decisions prey fish make affect their chances of survival (Weihs and Webb 1984, Soto et al. 2015). However, there are still serious gaps in our understanding the sensorimotor system functions during escape behaviors. In this introduction, I will give a brief overview about how prey fish use various sensory systems to detect an approaching predator, utilize their motor system to initiate and direct escape responses away from the predator, and how their escape response can strategically favor their survival.

Sensing predators:

Sensing predators in the environment is a vital ability for fish. In fact, a previous study has shown that larval fish who were able to respond before a predator initiated its strike had a three times greater chance of survival than larval fish who only reacted after the predator initiated its strike (Stewart et al. 2013). Furthermore in this study, larval fish that did not respond at all did not survive the predatory strike. This study demonstrates that it is vital for a prey fish to be able to detect threats quickly. Additionally, the sensory system and the associated information processing centers in the brain (as known as integration centers) must be able to determine the predator's bearing relative to its own position in space to help direct the prey's escape response away from the predator.

The visual system is denoted as the dominant sensory system for fish and is used to evade predators (Dill 1974, Webb 1982). Prey fish receive visual stimuli by collecting photons (a discrete units of light) with their eyes (Moyes and Schulte 2006). Photons are transduced to neural signals via photoreceptors in the retina and are processed in the optic tectum, the integration center for visual information (Dunn et al. 2016). One great benefit of the visual system is its near 360° field of view in most fish species (Fernald 1988). This means there is only a small region around a prey fish that predators can approach undetected by the visual system. Furthermore, due to the nature of photon emission, fish can detect threats at relatively far distances (Johnson 2012). This makes vision quite useful for detecting the predator early in the predator's approach, giving the prey ample time to react. The disadvantage to vision is its lengthy information processing delays that average about 200 ms (Burguess and Granato, 2007). Additionally, visually evoked escape responses can also have long delays since neural signals must travel down relatively complicated neural pathways to innervate muscles (Koyama et al. 2016). Though the detriments of the visual system may diminish the benefits of the visual system, the far-reaching sensing of the visual system can definitely enhance prey fish survival.

In close proximity or in low light situations, the lateral line system serves as a rapid, but limited sensory system. The lateral line system is a mechanosensory system that detects water flows close to the body of the fish. It is comprised of a network of neuromasts that spread across the epidermis of the fish, evenly patterned over the whole body (McHenry and Liao 2011). Neuromasts are small cylindrical structures that deflect with water flow, activating hair cells found within the neuromast. As the hair cells activate, neural signals are sent through afferent neurons that can immediately trigger escape responses (Eaton et al. 1991). This direct connection to motor pathways allows fish to trigger an escape response within 6 ms of hair cell activation,

3

making lateral line evoked escape responses at least an order of magnitude faster than visually evoked escape responses. In close proximity, approaching predators create fluid disturbances that propagate through the water (Stewart et al. 2014). These fluid disturbances can be detected by the lateral line system and be used to evoke an escape response. The lateral line system displays opposing set of benefits and detriments to the visual system. While the lateral line system can quickly process sensory information and initiated an escape response, the sensing range of the lateral line system is quite limited. Fluid disturbances that prey fish can detect decay exponentially from their source, making it difficult for prey to sense fluid disturbances that are far from its source (Stewart et al. 2014). Regardless of its limited sensing range, the lateral line system is still critical for prey survival in dark or turbid environments (Stewart et al. 2013).

Regardless of the sensory system, fish must decipher the sensory information to formulate an escape response. As prey fish sense their environment, they are constantly sampling their environment for threats. Prey fish will only initiate an escape response given a specific sensory cue (Tinbergen 1951). The visual cue that elicits an escape response is still unclear. Several studies have tried to elucidate what the visual-triggering cue could be for fish (Dill 1974, Temizer et al. 2015, Dunn et al. 2016), but there has not been one definitive answer. Many studies conclude that some aspect of the looming stimulus (the expanding image of the predator seen by the prey fish) triggers an escape response. There has been no clear fluid flow-triggering cue for the lateral line system either. However, how sensory information influence the prey fish's escape direction has been discerned. Studies have shown that the escape direction taken by a prey fish is related how the prey fish perceives the sensory information. For the lateral line system, larval zebrafish escape towards the side of their body that experiences a lower flow speed (Stewart et al. 2014). By following this scheme, larval zebrafish can escape away from the

4

predator since higher flow speeds occur closer to the moving predator. How visual cues affect escape direction will be discussed in the third chapter of the dissertation.

Escaping predatory strikes:

Once a prey fish has detected its threat and has recognized the direction it needs to escape towards, the prey fish escapes by performing a highly conversed escape response called a fast start. A fast start (otherwise known as a C-start or a startle response) is an escape response of fish that rapidly accelerates the fish towards a given direction (Weihs 1973). This response is ubiquitous among fish and is commonly used to escape threats. Fast starts are described in three sequential stages. In Stage 1, the fish unilaterally contracts its body, shaping the body into a 'C' shape. In Stage 2, the fish straightens its body and will accelerate rapidly towards a given bearing. Stage 3 is just defined as rapid undulatory swimming that occurs after the first tail beat of the fast start motion.

A complex network of neurons innervates muscles to generate the kinematics observed during a fast start. The Mauthner neurons (or M-cells), a bilateral pair of neurons, are the most prominent neurons in the fast start neural network and have been studied for over half a century (Korn and Faber 2008). During a fast start, only one of the two Mauthner neurons activates and creates a large electrical impulse that travels down the axon, while simultaneously inhibiting the other Mauthner neuron from firing. This impulse from the M-cell activates motorneurons on the contralateral side of the body. These motorneurons innervate skeletal muscles to create the Stage 1 kinematics (the initial 'C' shape). It is believed that Mauthner neurons are not responsible for conducting the neural commands that lead to Stage 2 motion, but rather that the neural command signal for Stage 2 are intrinsically connected to the Stage 1 neural command and are issued at the same time as the neural commands of Stage 1 (Eaton et al. 1988). This suggests that the whole

fast start commands (for at least Stage 1 and 2) are issued simultaneously, rather than sequentially.

The escape direction of an escape response is not purely dictated by Stage 1 kinematics. The escape direction is understood to be the sum of angular excursions taken in Stage 1 and 2 (Eaton et al. 1988, Foreman and Eaton 1993). For this reason, its important to understand how these two stages are controlled neurophysiologically. It is known that the Mauthner neurons do not necessarily dictate the overall escape direction the prey takes, but rather chooses whether the fish escapes towards the left or right side of its body. It has been hypothesized that there is a group of neurons (including the Mauthner neurons) that control the escape angle of a fast start; this group of neurons is called the brainstem escape network (Eaton et al. 1991). When the brainstem escape network initiates a fast start, the Mauthner neuron creates a large electrical impulse that overrides previous motor commands (Liu and Fetcho 1999). Simultaneously with M-cell activation, the other neurons in the brainstem escape network (thought to be the Mauthner homolog neurons) induce more detailed muscle activity to escape with a specific escape angle.

Strategies for escape:

Prey fish commit to an escape angle during an escape response. The decision to escape in a certain direction was determined by the prey's sensorimotor system. But do these decisions in escape direction enhance a prey's chance to survive a predatory encounter? This is more of a question of escape strategy, rather than of physiological mechanisms. However, through the course of natural history, escape strategies can affect prey physiology since natural selection favors escape strategies that promote survival (Domenici et al. 2011a). Therefore, it is worth discussing our current understanding of escape strategy.

For this introduction, an escape strategy determines the escape direction, otherwise known as the escape angle of an escape response. An escape angle is formally defined as the initial angle of escape the prey takes when it performs a fast start, relative to the approach of the predator. This means if a prey fish has an escape angle of 0°, then the prey will be moving in the same direction as the predator. Conversely, if the prey fish decides to escape with an escape angle of 180°, then the prey will be moving directly towards the predator. Determining what escape angle to take is not necessarily a simple or intuitive decision made by the prey. Escape angle decisions must consider many variables, such as position, velocity and other kinematic parameters. Currently, there are two opposing escape strategies for choosing escape angles: The optimal escape strategy and the protean strategy.

Optimal escape strategy:

The optimal escape strategy is based on a classic game theory model. It is a deterministic algorithm that states that given the ratio between the predator and prey's speeds, there is an optimal escape angle that maximizes the prey's chance of successful predator evasion. The optimal evasion strategy is based off a differential game theory model created in 1965 (Isaacs 1965) and then adapted for predator-prey interactions in 1984 (Weihs and Webb 1984). The main assumption in this model is that the prey's survivorship is maximized when the distance between the predator and prey is also maximized. In this model, the predator fish moves towards the prey, following a straight path towards the prey. As time progresses in the model ($t \rightarrow \infty$), the prey will evade the predator by escaping at a constant angle, α, away from the approaching predator. The following is a formula for the distance between the predator and the prey at it varies with time and α:

$$D^2 = ((X_0 - Ut) + Vt \cos \alpha)^2 + (Vt \sin \alpha)^2. \quad (0.1)$$

X_0 is the initial distance between predator and prey, while U and V are predator and prey speeds respectively.

As the predator charges the prey and prey escapes away at angle of α, there is a point in time where the predator and prey will be the closest together. This minimum distance between the predator and prey is called D_{min}. To maximize the prey's chance to evade a predatory strike, the prey wants to maximize D_{min} by adjusting α. The following is the equation for D_{min} as it varies with α, which was derived from Eqn. 0.1:

$$D_{min}^2 = \frac{\sin^2 \alpha}{K^2 + 2K \cos \alpha + 1}. \qquad (0.2)$$

In Eqn. 0.2, K is the ratio of U and V and D_{min}^2 is normalized by X_0.

From equation 2, the optimal escape angle, α, can be solved for, given value of K. If $K > 1$, the prey should escape with an escape angle following Eqn. 0.3:

$$\alpha = \cos^{-1}\left(\frac{1}{K}\right). \qquad (0.3)$$

Equation 3 shows that as the predator travels faster than the prey ($K \to \infty$), the prey can maximize the distance between the predator and itself if it can escape with an escape angle closer to 90°. When $K \leq 1$, the solution for α is more complicated. In fact, there is no single optimal escape angle, but rather an array of equally optimal escape angles (Soto et al. 2015):

$$|\alpha| \leq \cos^{-1}(K). \qquad (0.4)$$

Eqn. 0.4 describes that given a value of $K \leq 1$, α can range in value between $-\cos^{-1}(K)$ and $\cos^{-1}(K)$ and have an escape with an equally high chance of survival.

There are some weaknesses to this model. The authors themselves carried out experiments that measured escape angles respective to the predator approach to compare to the model (Weihs 1984). Though the calculated optimal angle falls within the range of values

observed in their experiments, the variance was too high to come to a solid conclusion of whether prey fish use an optimal escape strategy. Few studies try to corroborate this specific model with experimental measurements (Soto et al. 2015, Corcoran and Conner 2016) and have come to similar conclusions. This mathematical model also has some strict assumptions. This model assumes that both predator and prey have constant velocity and that prey fish are able to determine the predator's speed. These assumptions are probably broken in realistic settings, since predators usually decelerate before attempting to capture prey and prey rapidly accelerate when performing a fast start (Higham 2007). Also it is dubious that prey fish can precisely measure predator velocity, since that would require binocular vision, which prey fish do not often use when escaping predators (Dill 1974). Nevertheless, given the set-up of this theoretical model, an exact escape angle can be calculated; and till this date, there are no other mathematical models that make such a precise prediction, without borrowing principles and concepts from this model.

Protean escape strategy:

Another point of contention about the previous model is that if prey escape strategy follows a deterministic algorithm, such as the optimal escape strategy, then the prey's escape will become predictable. It has been hypothesized that if prey fish have the same deterministic strategy to evade predators, predators could then adjust their strategy to counter the unsurprising nature of a prey's escape through learning or natural selection (Domenici et al. 2011a). The tentacled snake (*Erpeton tentaculatus*) is an example of a predator that employs such a counter strategy (Catania 2009). Therefore, instead of a predictable escape angle, an alternative strategy is a protean approach to picking an escape angle. A protean strategy dictates that an escape angle should be randomly chosen (Humphries and Driver 1970). By employing a protean strategy, predators

cannot necessarily predict where prey will escape to, thwarting a predator's attempt to predict a prey's escape angle.

The protean escape strategy does have a trade-off. To maximize the unpredictability of an escape direction, prey fish must maximize the range of escape angles it uses to escape. At the very extreme case, this would imply that prey should have an equal chance of escaping in every possible direction, including escape paths pointing towards the predator, which could be a counterproductive for prey survival. Similar to the previous theoretical model, the use of the protean strategy in nature is hard to corroborate with data collected in the field and in experiments.

Current Dissertation

For this dissertation, I used zebrafish (*Danio rerio*) as a model organism for predator-prey interactions. The larval stage of this species serves as a model for studying the neurophysiological (Huang et al. 2013, Bagnell and McLean 2014, Bianco and Engert 2015) and biomechanical (Müller and van Leeuwen 2004, Li et al. 2016) basis of behavior. Predator-prey interactions can be experimentally replicated in the lab, where adults strike at larvae with suction feeding and the larvae respond with a fast-start escape response (Stewart et al. 2013). These are the two principle behaviors that characterize a broad diversity of piscivorous interactions (Weihs and Webb 1984, Walker 2005).

My dissertation is comprised of three studies that further our understanding of predator-prey interactions. The chapters in this dissertation further detail the sensorimotor basis for escape in larval zebrafish. With my work, I have built a framework for understanding fast starts with three-dimensional escape trajectories, evaluated the importance of sensory and motor system for prey survival, and created a new way of understanding escape strategies that combined ideas

from two, once-opposing schools of thought on predator evasion. Together, this dissertation gives a holistic perspective on predator evasion in fish species and the underlying sensorimotor system that governs it.

CHAPTER 1: Zebrafish larvae use fast starts to locomote in three-dimensional maneuvers

Introduction

Fish evade predators by executing a 'fast start' escape response that is rapid, yet permits swimming in a controlled direction (Domenici and Blake 1997). This behavior enables a fish to survive an encounter with a predator (Walker et al. 2005). However, it remains unclear what mechanics and neurophysiology facilitate this directional control. Zebrafish larvae (*Danio rerio*) present unique opportunities to test hypotheses on this subject, but the morphology of larvae is distinct from adults and they are at least an order of magnitude smaller. Therefore, larval fish have the potential to deviate from the adult models of neuromechanical control (e.g. Foreman and Eaton 1993). One feature that has not been reported for adult fish is the ability of larvae to control the elevation of a fast start. Elevation is the angular deviation from the horizontal plane in an earth-bound frame of reference and its control allows larvae to dive away from a predator (Stewart et al. 2014). In the interest of understanding how motor systems facilitate this control, the present study measured the three-dimensional (3D) kinematics of larval zebrafish when executing fast starts that vary in elevation.

The fast start is a classic behavior for studying motor control in vertebrates. Escape responses like the fast start were thought to operate as a 'fixed-action pattern' with stereotyped kinematics that are initiated by a threshold stimulus (Barlow 1968). Consistent with this idea, the fast start follows a characteristic sequence that has been described in three stages. In stage 1, the fish unilaterally contracts its muscles, which bends the body into a 'C' shape and causes the head to yaw. In stage 2, the head rotates in the opposite direction through the action of contralateral muscles, as the body straightens and accelerates forward. This is followed by the rapid

undulatory swimming of stage 3 (Weihs 1973). Variation in the speed and degree of body

rotation within each of these stages generates escape kinematics with a variable azimuth, which

is the angular heading on the horizontal plane. The azimuth has been shown to depend on the

intensity and direction of a stimulus (e.g. Eaton et al. 1981, Peterson 1984, Eaton et al. 1988,

Nissanov et al. 1990, Eaton et al. 1991, Liu and Fetcho 1999). Therefore, the fast start exhibits a

degree of control that is beyond the stereotyped motion of a fixed- action pattern.

Ideas about the directional control of the fast start are largely based on research on adult

goldfish (*Carassius auratus auratus*). These studies have demonstrated that the fish rotates away

from a threat anterior to the body by first creating a large stage 1 yaw. This is followed by less

rotation in the opposite direction during the acceleration of stage 2. In contrast, a caudal stimulus

generates a relatively modest yaw over both stages to direct swimming forward (Eaton et al.

1988, Eaton and Emberley 1991). As a consequence of these patterns, the azimuth of an escape

is correlated with the yaw angles generated in stages 1 and 2. This is an observation that is

consistent with the hypothesis that the reticulospinal neurons that control a fast start are activated

in a manner that depends on the relative position of a stimulus (Foreman and Eaton 1993).

Zebrafish larvae offer opportunities to test these ideas with visualization techniques that

have benefited from the transparent bodies of these animals. For example, calcium imaging

revealed that three reticulospinal neurons are activated by a rostral stimulus, whereas only one

neuron is activated by a caudal stimulus (O'Malley et al. 1996). These results support the control

model that was based on adult goldfish (Foreman and Eaton 1993). Further opportunities in this

area are developing with a growing toolkit of transgenic lines for zebrafish that permit functional

imaging and optogenetics (e.g. Fetcho et al. 2008, Nakayama and Oda 2004, Akerboom et al.

2012). Despite these advances, fundamental aspects of the behavior remain unresolved for larval

fish and it is not clear how the body moves to direct the fast start in three dimensions (Müller and van Leeuwen 2004, Stewart et al. 2014). It is for these reasons that the present study aimed to measure the 3D body kinematics of zebrafish larvae for fast starts that vary in direction.

Materials and Methods

We used kinematic measurements to describe the body motion of larval zebrafish. In particular, the rotation of the head and bending of the tail were measured from high-speed recordings of fast starts that were stimulated with a jet of water. We examined how these measurements correlated with the direction of the escape trajectory in azimuth and elevation. These findings offer an observational basis for understanding how larval fish control fast start direction in three dimensions.

Animal husbandry

All experiments were performed on zebrafish larvae (*Danio rerio*, Hamilton 1822) between the ages of 5 and 7 days post-fertilization. All larvae were bred from wild-type (AB line) colonies housed in a flow-through tank system (Aquatic Habitats, Apopka, FL, USA) that was maintained at $28.5°$C on a 14 h:10 h light:dark cycle. The fertilized eggs from randomized mating were cultured according to standard techniques (Westerfield 1993).

Experiments

We recorded the 3D kinematics of escape responses with two high-speed video cameras. Larvae were recorded in an acrylic tank (a 30 mm cube) with the cameras positioned above the surface and normal to one of the walls. The cameras (FASTCAM 1024PCI, Photron, San Diego, CA, USA) recorded at 1000 frames s^{-1} and were synchronized with a transistor–transistor logic (TTL)

pulse. Larvae were visualized with transmitted illumination that was provided by two high-power LED floodlights (120 W equivalent daylight, 5000K PAR38 dimmable LED flood light bulb, Philips, Andover, MA, USA) with diffusers (100 mm × 100 mm opal glass, Edmund Optics, Barrington, NJ, USA).

Zebrafish were induced to direct their escape in a variety of directions with a fluid jet. After a 15 min acclimation period, we exposed larvae to this stimulus, which was emitted from a curved capillary tube with an inner diameter of 1.1 mm. We directed this tube towards the center of the tank and positioned it either above or below the larvae. The impulsive pressure (Picospritzer II, General Valve Corporation, Fairfield, NJ, USA) was adjusted to have a 7 ms duration and a peak pressure of 14 kPa. These settings were sufficient to elicit a reaction from the larva but not displace the body.

Kinematic analysis

We performed a calibration to resolve 3D coordinates from the recordings by the two cameras. The calibration used recordings of a calibration body of a known geometry that was placed in the center of our water-filled tank. This body contained 27 distinct landmarks of known 3D position, which we designed with CAD software (SketchUp 2013, Trimble Navigation, Sunnyvale, CA, USA) and created with a 3D printer (ShapeWays, New York, NY, USA). The calibration was performed by a direct-linear transformation (Digitizing Toolkit, Hedrick, 2008) in MATLAB (version 2014a, MathWorks, Natick, MA, USA) from manually selected coordinates at landmarks on our calibration body from the two camera recordings.

Two-dimensional position data were collected from both cameras to reconstruct the 3D motion of a larva. Using custom software developed in MATLAB, the 2D coordinates from both views were collected from the body landmarks for each frame of both recordings. Software

developed in MATLAB was further employed to implement all of the post-processing and statistics described below. The body landmarks consisted of the centers of both eyes and the posterior margin of the swim bladder. For the tail, we recorded a series of positions (8–20 points, depending on the curvature of the tail and the perspective of the camera) along the dorsal and ventral edges, which were visible because of lines of pigmentation. Position data were smoothed with splines that were implemented with a least-squares approximation ('spap2' in MATLAB) with user-defined knots to compensate for calibration error and inconsistencies in the acquisition of body landmarks. Splines were fitted to the time series of each dimension of the data for the eyes and swim bladder, as well as the spatial variation of the tail coordinates for each video frame.

We determined the rotation of the body from our measurements of the position of the head. This was achieved by defining a coordinate system with its origin at the mean position between the eyes. The y-axis of this system was directed to the right side of the body and was calculated as a unit vector that was directed from the origin to the right eye. The z-axis was calculated as the cross product of y-axis vector and another running from the origin to the swim bladder. Finally, the x-axis was determined from the cross product of the y and z-axes. Angular changes in this coordinate system were defined as the Euler angles of roll, pitch and yaw, which indicated rotation around the x, y, and z-axes, respectively. Euler angles were calculated from 3×3 rotation matrices defined with respect to the body orientation prior to the initiation of the fast start (Craig 1989).

The timing of each stage in the fast start was determined by oscillations in yaw (Fig. 1.1D - F). Stage 1 was defined as the duration between the onset of motion and the first maximum or minimum of yaw, when the body curled into its initial 'C' shape. Stage 2 spanned from the end

of stage 1 until the next minimum or maximum in yaw as the body unfurled. This was followed by stage 3, which continued up to the third maximum or minimum value in yaw, as the larva undulated its body for half of a tail beat. Changes in the Euler angles were defined as the angular difference between these angles from one stage to another. The changes in Euler angles associated with different directions for the escape trajectory were statistically compared using a one-way ANOVA (comparing up, down and lateral directions) or a t-test (comparing left and right turns). Outliers were excluded from statistical tests and were determined by a two standard-deviation cut-off.

The direction of an escape was calculated from the trajectory of the swim bladder over stages 2 and 3. The posterior margin of the swim bladder approximates the body's center of mass (Stewart and McHenry 2010) and therefore offered a measure of the prevailing direction of body motion. We found the trajectory direction by a 3D linear, least-squares fit of the position recordings between the start of stage 2 and end of stage 3. From this vector, we calculated the azimuth and elevation of the trajectory. Azimuth and elevation angles were respectively compared with changes in yaw and pitch using linear regression analysis.

We determined the motion of the tail from changes in its orientation. We solved for 19 points of even spacing along the arclength from each spline-fit for the dorsal and ventral margins of the tail. The line segments between each pair of points for the dorsal and ventral margins were used to define a 3D plane that represented the orientation of a segment of the tail. We derived the angular excursion of this plane in lateral and dorsoventral orientations relative to the orientation of the same segment prior to the fast start.

Results

Body rotation

Zebrafish larvae exhibited all three stages of the fast start within view of both cameras. Using the posterior margin of the swim bladder to approximate the center of mass (Stewart and McHenry 2010), we found that the body of a larva curled into a 'C' shape during stage 1 with little center-of-mass translation. The body then began to displace as it unfurled in stage 2, in the transition towards the undulatory swimming of stage 3 (Fig. 1.2A). The durations of each stage were statistically indistinguishable (one-way ANOVA: $P = 0.70$, $n = 15$), with each lasting about 8 ms (7.76 ± 2.08, mean $\pm$ 1 SD, $n = 15$, Fig. 1.2B).

From the beginning of a fast start, the larvae rotated their body in the direction to which they were ultimately headed. This was indicated by our measurements of the Euler angles (yaw, pitch and roll, Fig. 1.1A), which were calculated from the coordinates of the eyes and swim bladder. For example, a larva moving downwards and towards the left side of the body (teal curves in Fig. 1.1B - C) showed changes in yaw and pitch that progressively grew more negative across all stages of the fast start (Fig. 1.1D - E), which was consistent with the convention of our coordinate system (Fig. 1.1A). The trend in pitch was apparent in stage 1, which indicates a directional bias that started at the earliest moments of an escape. This may be contrasted with an escape that remained largely on a horizontal plane (e.g. dark blue curves in Fig. 1.1B - C). Whilst also showing short-period and large- amplitude oscillations in yaw (Fig. 1.1D), the pitch angle of this response did not trend away from a zero value (Fig. 1.1E). Regardless of the direction of a trajectory, larvae exhibited roll that could be comparable in magnitude to pitch, but we found no evidence that these changes were associated with the direction of the escape (Figs 1.1F and 1.3C).
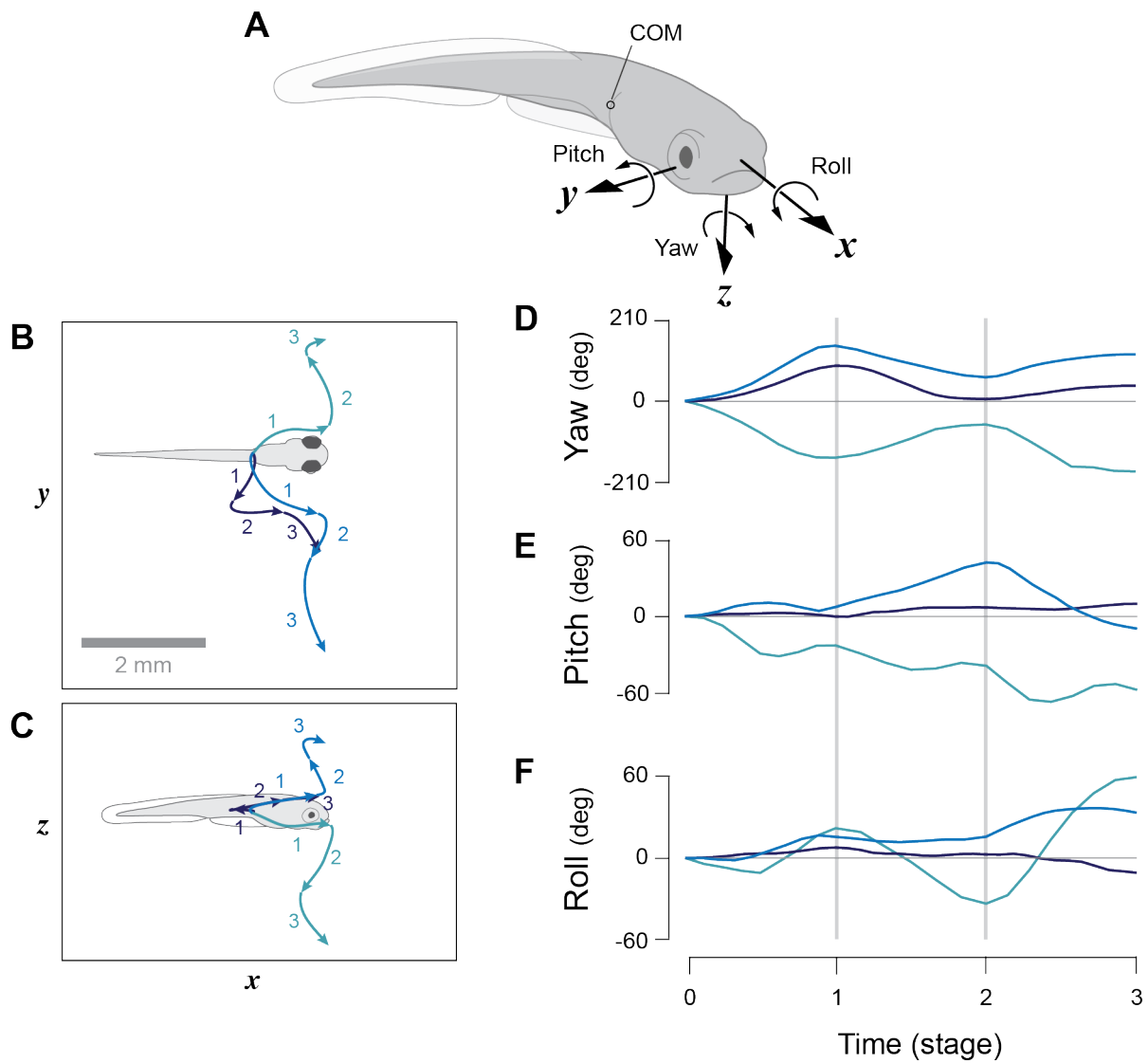
Fig. 1.1. Three-dimensional trajectories of the fast start in zebrafish larva. (A) A schematic diagram of the coordinate system used for the body of a larva with its Euler angles. The body's center of mass (COM) was approximated at the posterior margin of the swim bladder (Stewart and McHenry, 2010). (B - C) Trajectories of the COM during the fast start in three different directions on a horizontal (x–y) plane (B) and a vertical (x–z) plane (C). The Euler angles of the sequences shown in B and C are shown in terms of yaw (D), pitch (E) and roll (F).

19
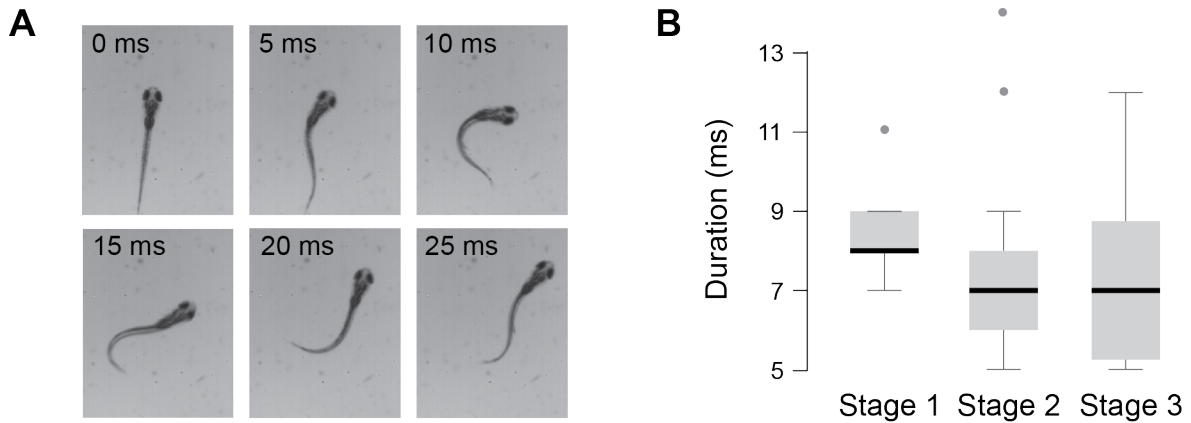
Fig. 1.2. The stages of a fast start. (A) Video frames of a representative fast start, recorded from a dorsal view in 5 ms intervals. A fast start is described in three stages. In stage 1, the zebrafish larva curls its body to one side, then rapidly unfurls its body in stage 2 and begins undulatory swimming away in stage 3. (B) All stages were statistically indistinguishable in duration (one-way ANOVA, $P = 0.70$, $n = 15$). The durations of each stage are shown with a box- and-whisker plot with the median (black line), first and third quartiles (gray box), range (whiskers) and outliers (filled circles, > 2 SD).

Yaw and pitch varied with the escape direction. For example, fast starts to the left were characterized by a negative change in yaw for stage 1 (Fig. 1.3A), because the body initially curled in the ultimate direction of the trajectory (Fig. 1.1A). This was followed by a positive change in yaw during stage 2 and another reversal in stage 3 (Fig. 1.3A). In each of these stages, the differences in yaw were highly distinct (t-test: $P < 0.001$, $n = 15$) between escapes to the left and right. In a similar way, fast starts directed upwards, laterally and downwards were all significantly different in the changes in pitch achieved in each stage (one-way ANOVA: $P < 0.001$, $n = 15$, Fig. 1.3B). In contrast, body roll did not vary significantly between escapes of different direction (one-way ANOVA: $P > 0.05$, $n = 15$, Fig. 1.3C).

The azimuth and elevation angles of a trajectory were correlated with the rotations of the head. In particular, change in the yaw angle was correlated with the azimuth of the trajectory for stage 1 ($P < 0.001$, $r^2 = 0.71$, $n = 15$), but not in subsequent stages (Fig. 1.4B). The change in pitch for all stages was correlated with the elevation ($P < 0.001$ for stages 1 and 2, $P = 0.046$ for stage 3, $n = 15$). As indicated by the coefficient of determination, most variation in elevation could be predicted from differences in the change in pitch over stages 1 ($r^2 = 0.87$) and 2 ($r^2 = 0.68$, Fig. 1.4C). Only about one- third of the variation in elevation could be predicted from the change in pitch over stage 3 ($r^2 = 0.27$). Therefore, the degree of elevation change created during a fast start is closely related to body pitching in the first two stages.
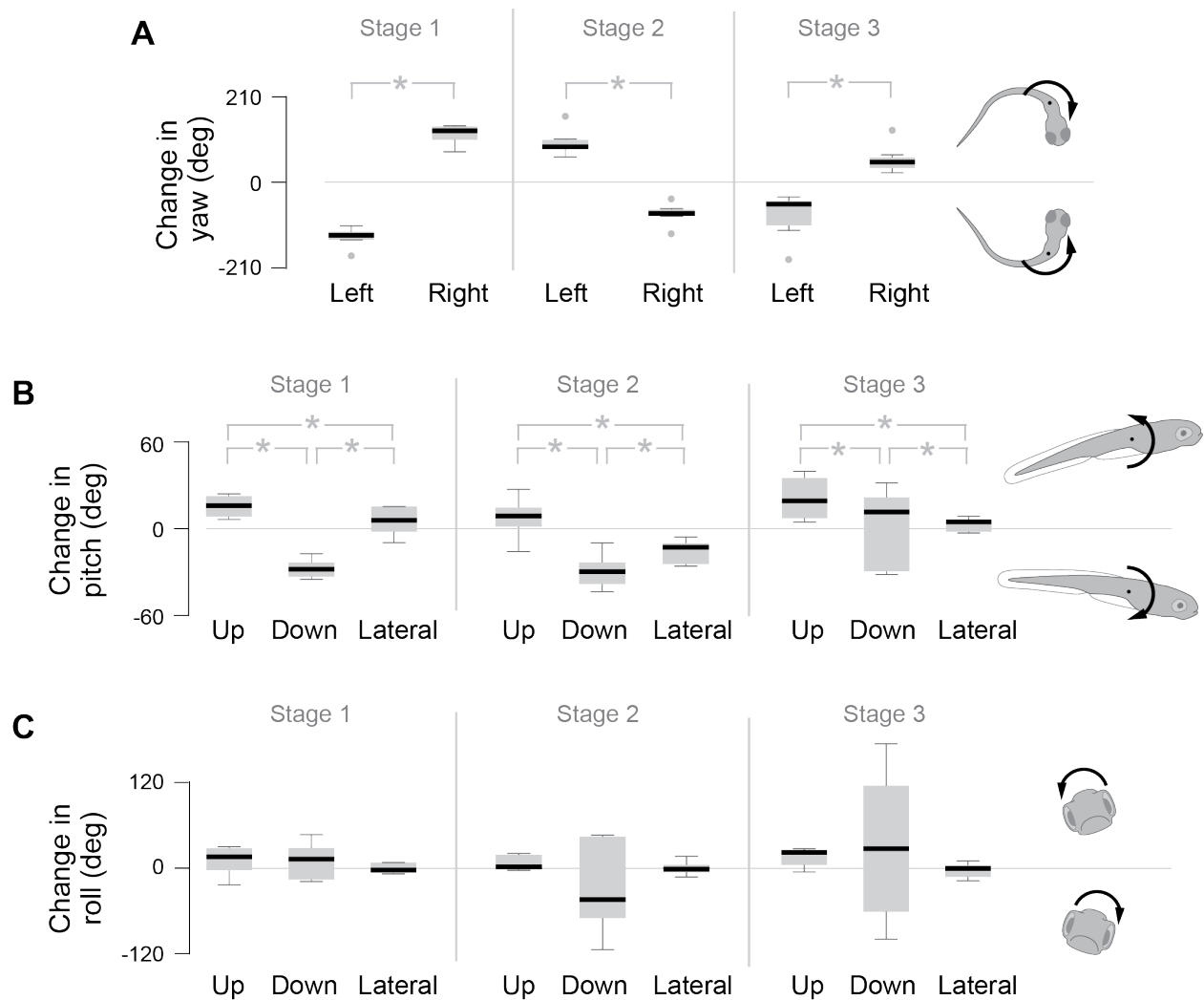
Fig. 1.3. Body rotation for fast starts in different directions. We measured body rotation by change in the Euler angles during each stage of the fast start. (A) Change in yaw differed significantly between fast starts that were directed to the left or right of the body for all stages ($P < 0.001$, $n = 15$). (B) Change in pitch differed significantly between fast starts that were directed upwards, downwards and laterally (within $\pm 15°$ margin) from the initial orientation for all stages ($P < 0.001$, $n = 15$). (C) Change in roll had no significant differences between upward, downward and lateral fast starts. Each group of measurements is presented by its median (black line), first and third quartiles (gray box), range (whiskers) and outliers (filled circles, > 2 SD), with significant differences (*) between groups.
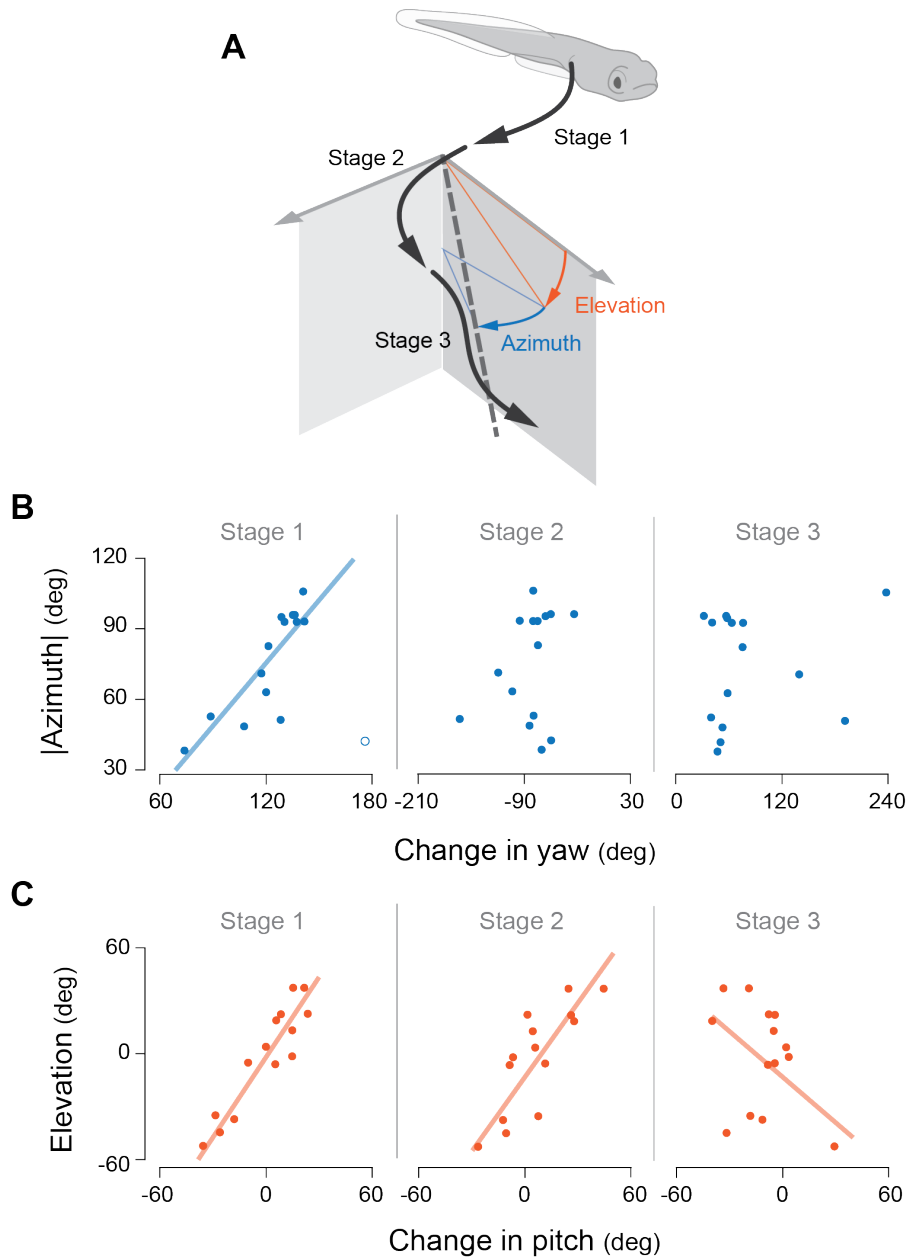
Fig. 1.4. The relationship between body rotation and the direction of a fast start. (A) The azimuth (in blue) and elevation (in red) of the fast start trajectory were found with a least-squares linear fit of the trajectory of stages 2 and 3. (B) Correlations between changes in yaw and the absolute value of the azimuth angle were significant for stage 1 ($P < 0.001$, $r^2 = 0.70$, $y = 0.94x - 37.2$, $n = 15$). (C) In contrast, changes in pitch for each stage were significantly correlated with the elevation of a fast start ($P < 0.001$ for stage 1, $y = 1.51x - 1.85$ and stage 2, $y = 1.40x - 12.4$; $P = 0.046$ for stage 3, $y = -0.86x - 12.8$, $n = 15$). In addition, the changes in pitch during stage 1 ($r^2 = 0.86$, $n = 15$) and stage 2 ($r^2 = 0.68$, $n = 15$) were highly predictive of variation in elevation. In contrast, change in pitch during stage 3 predicted only about one-third of variation in elevation ($r^2 = 0.27$, $n = 15$). Outlier values are presented as open circles.

23

Tail kinematics

We measured tail kinematics to examine how the bending of the body related to head rotation and the direction of a fast start. From coordinates of the dorsal margin of the tail, we measured the angular excursion relative to the initial orientation of the body in the lateral (Fig. 1.5A) and dorsoventral (Fig. 1.5B) directions. This provided the means to relate tail motion to the Euler angles of the head (Fig. 1.1A) and offered a measurement of bending with a superior signal-to-noise ratio than calculations of tail curvature. This allowed us to examine how the rapid change in the lateral excursion of the head (i.e. yaw, Fig. 1.1A) was reflected in the angular excursion of the tail (Fig. 1.5C) with a delay. A similar pattern was apparent in the dorsoventral excursion, where changes in the head (i.e. pitch, Fig. 1.1A) were reflected with a delay in the tail (Fig. 1.5D). Therefore, the tail followed a course of motion set by the head in both lateral and dorsoventral directions. Head rotation was also related to simultaneous change in the angular position of the tail in the opposite direction. This was most acute in stage 1, where positive changes in the lateral excursion of the head were mirrored by negative changes in the tail with lower magnitude (Fig. 1.5C).

The propagation of undulatory waves in the tail differed between escapes towards the left and right. For example, in a rightward fast start (Fig. 1.6Ai), the anterior region of the tail followed a positive (i.e. clockwise from a dorsal view) angular excursion (Fig. 1.6Bi) as the head yawed towards the right of the body (Fig. 1.6Ci) during stage 1. At this time, the posterior region of the tail bent in the opposite direction, with a negative (i.e. counter-clockwise) angular excursion (Fig. 1.6Bi). The end of stage 1 was marked by a reversal in yaw and the tail excursion created by the unfurling of the body from this stage. Undulatory waves generated similar reversals in excursion, which marked the ending of stages 2 and 3 (Fig. 1.6Bi).

A Lateral excursion

B Dorso-ventral excursion

C

Stage 1   Stage 2   Stage 3

Lateral excursion (deg)

D

Dorso-ventral excursion (deg)

Time (ms)
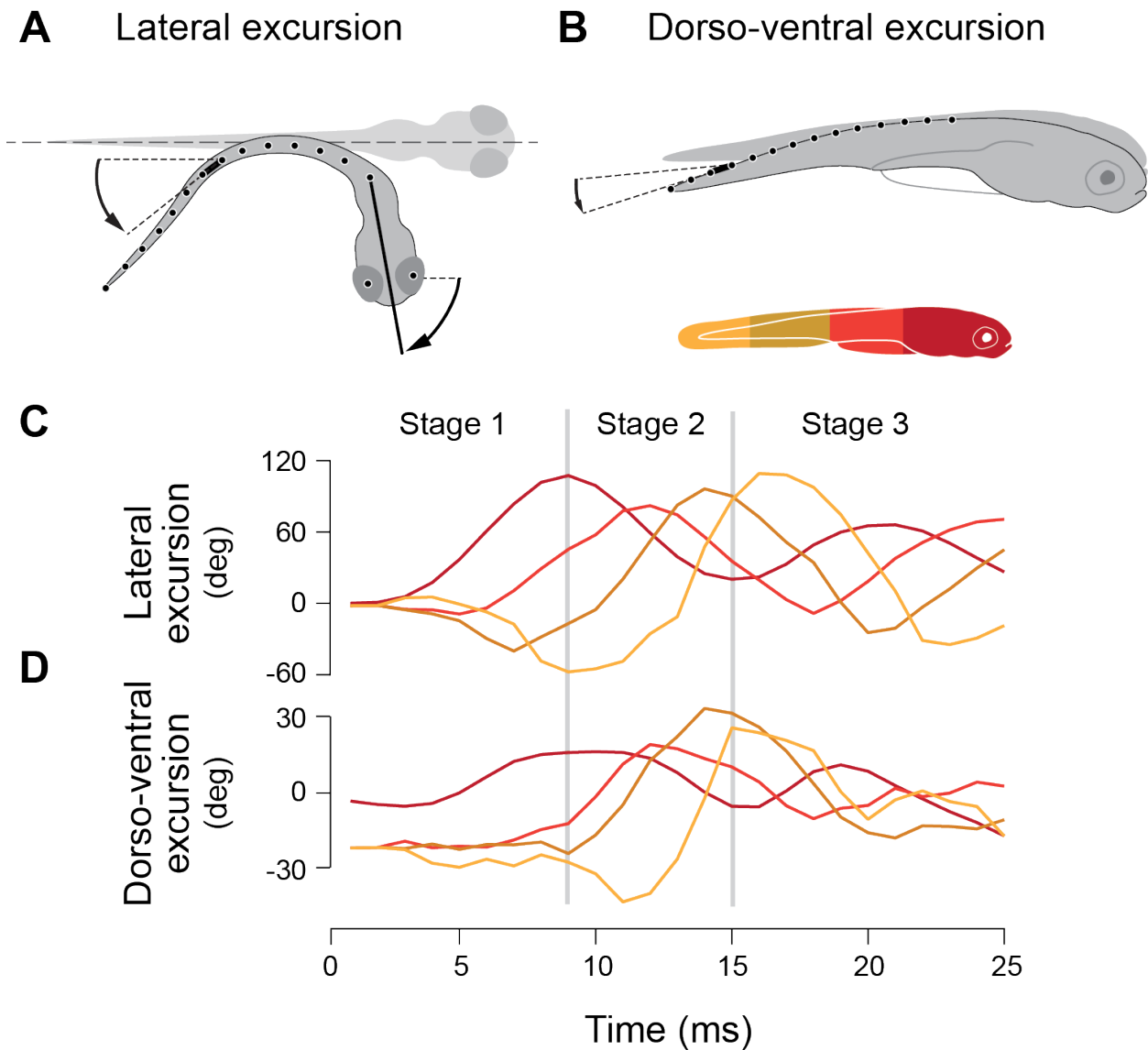
Fig. 1.5. Body bending during a fast start. Angular excursions of the head and tail show rotation of the body relative to the initial orientation of the body in lateral (A) and dorsoventral (B) directions. (C-D) Rotation of the head (in dark red) has been plotted over time with tail angular excursion from the anterior ($0 < L < 0.25$, in orange), middle ($0.25 < L < 0.50$, in gold) and posterior ($0.50 < L < 0.75$, in yellow) regions for one fast start in lateral (C) and dorsoventral (D) directions.
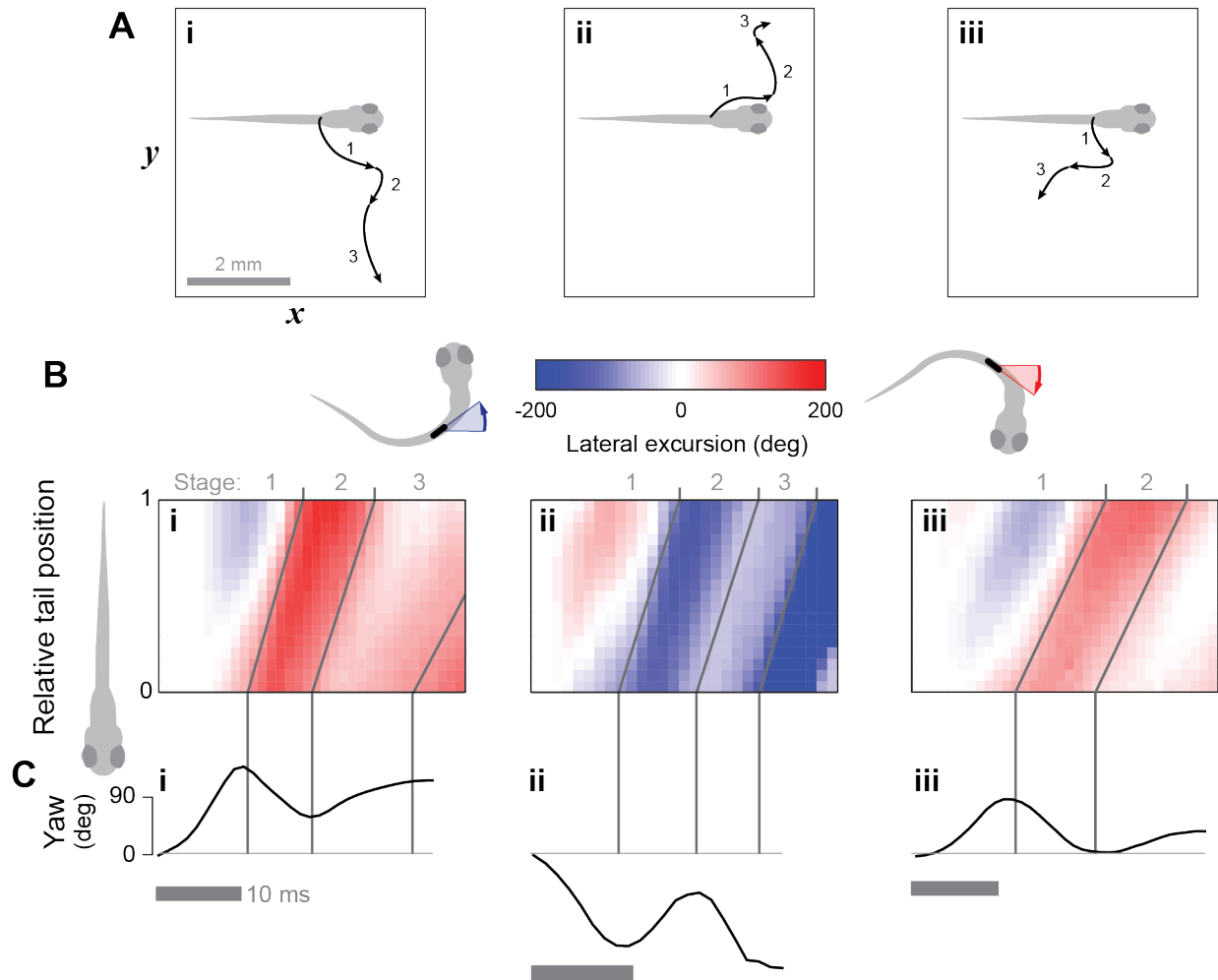
Fig. 1.6. Lateral bending during a fast start. The lateral tail excursion and yaw for fast start maneuvers directed towards the right (i and iii) and left (ii) of the body (the same sequences as in Fig. 1.1B – F). (A) The trajectories for each fast start is plotted in the horizontal plane, with arrows presenting the trajectory achieved over an individual stage. (B) From the same three fast starts depicted in A, we measured the lateral excursion of the tail, throughout its length in pseudocolor that encodes positive (in red) and negative (in blue) angles. Diagonal lines (dark gray) in each pseudocolor plot denote the transition between the stages of each fast start. (C) The corresponding measurements for the yaw of the head are shown for the same sequences as illustrated in A and B.

An escape towards the left side of the body (Fig. 1.6Aii) showed a similar pattern, but in the opposite direction (Fig. 1.6Bii, Cii).

Similar differences in bending were apparent in the dorsoventral direction among responses that varied in elevation. For example, an escape upwards (Fig. 1.7Ai) began with a dorsal bend in the tail (Fig. 1.7Bi), as the head pitched in the same direction (Fig. 1.7Ci). The end of each stage was marked by undulatory waves in dorsoventral excursion that were initiated by the motion of the head. Similar events occurred in escapes directed downwards, but in the opposite direction (e.g. Fig. 1.7Aii, Bii and Cii). An escape trajectory that was restricted to planar motion (Fig. 1.7Aiii) occurred with relatively minor variation in pitch (Fig. 1.7Ciii) and dorsoventral angular excursion (Fig. 1.7Biii). Therefore, the dorsoventral motion of the tail largely propagated from the pitching apparent in the motion of the head at each stage in the fast start.

We examined relationships between the extent of the tail's angular motion and the direction of the fast start. We found significant correlations ($P \ll 0.001$, $n = 15$) between the lateral excursion of the posterior region of the tail ($0.9L$, where L is the length of the tail) and the azimuth of the trajectory for all three stages (Fig. 1.8A). We similarly found significant correlations ($P < 0.001$, $n = 15$) between the change in dorsoventral excursion of each stage and elevation for the posterior region (Fig. 1.8B). The anterior region was also significantly correlated with elevation for stages 1 and 2. These correlations with elevation were positive for the anterior region, where the tail rotated in the same direction as the head and ultimate heading of the trajectory. The negative correlations for the posterior region were the result of the tail rotating in the opposite direction during bending (Figs. 1.5D, 1.7). Therefore, the angular excursion of the tail was found to be predictive of the direction of a fast start.
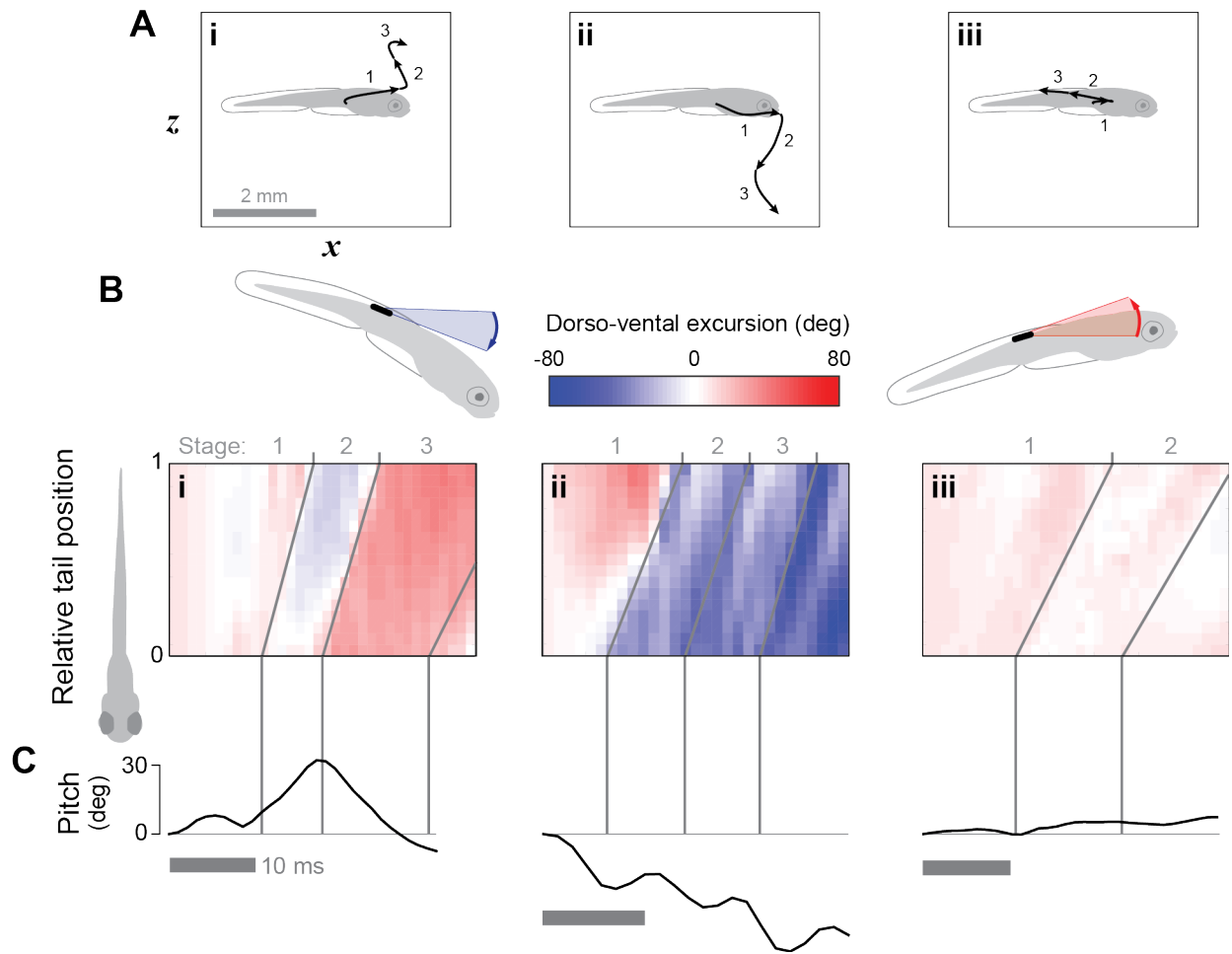
Fig. 1.7. Dorsoventral bending during a fast start. (A - B) The dorsoventral excursion during fast starts directed (i) upwards, (ii) downwards and (iii) laterally (the same sequences as in Fig. 1.1B - F and Fig. 1.6). (A) The trajectory for each fast start plotted in the vertical plane with arrows that differentiate each stage. (B) The dorsoventral excursion of the body changes with bending that is directed downwards (in blue) and upwards (in red). Diagonal lines (dark gray) in each pseudocolor plot denote the transitions between the stages. (C) Measurements of the corresponding pitch angle for the head are shown for the same sequences as illustrated in A and B.
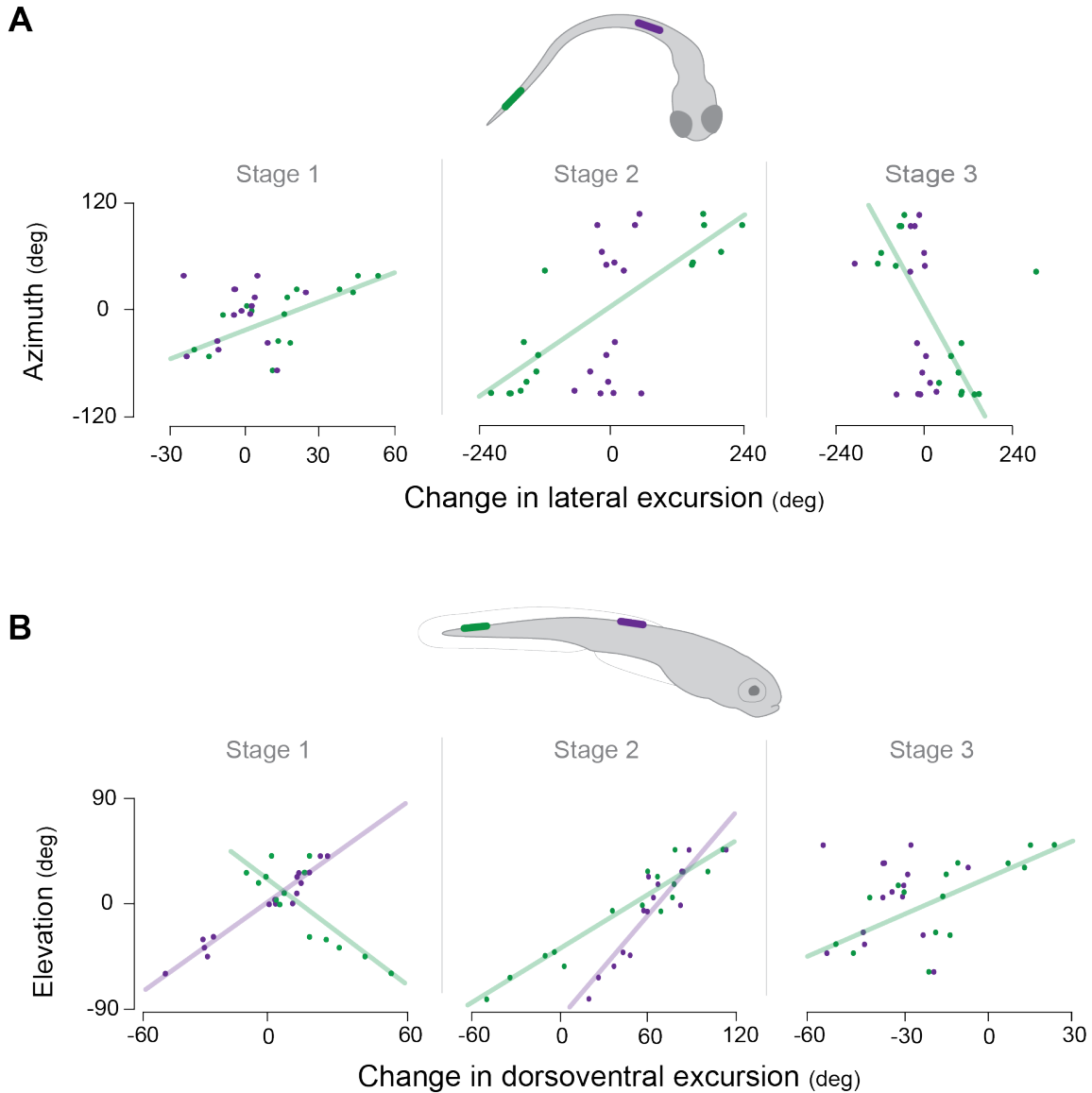
Fig. 1.8. The relationship between body bending and the direction of a fast start. The total angular excursion for the tail in the anterior (0.1*L*, in purple) and posterior (0.9*L*, in green) region of the tail in the lateral (A) and dorsoventral (B) directions for the stages of numerous (*n* = 15) fast starts. (A) We found a significant correlation ($P \ll 0.001$) between the lateral excursion of the tail and the azimuth of the escape trajectory for the posterior (0.9*L*, in green) region of the tail during stage 1 ($y = 1.48x + 11.5$, $r^2 = 0.90$), stage 2 ($y = 0.428x + 2.86$, $r^2 = 0.85$) and stage 3 ($y = 0.56x - 19.6$, $r^2 = 0.81$). (B) Variation in the elevation of an escape could be well predicted from the dorsoventral excursion of the tail. Correlations were significant ($P < 0.001$) for both regions of the tail and for all stages of the fast start for stage 1 (anterior: $y = 1.40x + 0.78$, $r^2 = 0.65$; posterior: $y = -1.48x + 11.5$, $r^2 = 0.96$) and stage 2 (anterior: $y = 1.58x + 0.34$, $r^2 = 0.85$; posterior: $y = 0.83x + 10.9$, $r^2 = 0.90$). The dorsoventral excursion of the posterior of the tail only explains about half the variation in elevation ($y = 1.06x - 22.8$, $r^2 = 0.49$).

29

Discussion

Larval zebrafish vary the direction of a fast start in a manner similar to adult fish, but can execute this maneuver in three dimensions. The ability to control their escape trajectory in elevation is compatible with current thinking about the motor control of the fast start, but requires an additional means for control. Our measurements offer a basis for considering the neurobiology and biomechanics of this 3D directional control in larval fish.

The kinematics of a 3D fast start

Larval zebrafish vary the azimuth of a fast start with kinematic differences that are similar to adult fish. Adult goldfish show a positive correlation between yaw in stage 1 and the azimuth escape angle of a fast start (Eaton et al. 1991), which is similar to our results (Fig. 1.4B). Our findings are also consistent with the observation that a rostral stimulus creates larger head yaw and a greater change in direction than a caudal stimulus in both larval (Liu and Fetcho 1999) and adult fish (Foreman and Eaton 1993). Although zebrafish larvae can exhibit a comparable change in yaw during stage 1 (Fig. 1.4B), the maximum azimuth angle that can be attained is smaller than in adults. Despite such differences, which are likely to stem from scale-dependent mechanics, both larvae and adults turn left or right to a greater degree by yawing more in stage 1. This common feature in kinematics justifies the use of larval fish to study the neuromechanical mechanisms of control in all fishes.

The elevation of a fast start in larvae is related to dorsoventral motion of the head and tail. During stages 1 and 2, nearly all variation in elevation can be predicted from changes in the pitch angle of the head (Fig. 1.4C). Therefore, as the head yaws laterally in stage 1, it simultaneously pitches towards the elevation of the maneuver's heading (Fig. 1.4C). This pitching motion occurs when the tail bends to momentarily form a shallow 'C' shape that is

concave towards the dorsal or ventral directions. The degree of this dorsoventral bending varied with the elevation of the trajectory, as indicated by the angular excursion of the tail (Fig. 1.8B). In contrast to the oscillations in yaw that correlate with the azimuth of the escape, the pitching of the head proceeds in a similar direction throughout the three stages of a fast start (Figs 1.2, 1.4).

These kinematics may be summarized by the events in each stage for a particular fast start. Consider a case where a larva dives down and to the left (Fig. 1.9A) with direction motion that begins in stage 1. As the body curls together, the head pitches downwards and he tail bends in a concave-ventral direction. Therefore the combined pitch and yaw of the head in stage 1 sets the body in the general direction of its ultimate heading (Fig. 1.9A - B). During stage 2, the head reverses direction in yaw, but its pitching continues along a downward path (Fig. 1.9C). This will continue into stage 3 as the head continues to oscillate in yaw (Fig. 1.9D).

Our measurements indicate that zebrafish larvae are capable of executing a fast start with substantial 3D motion. This was reflected in the elevation of the trajectory, which spanned almost $60°$ both upwards and downwards (Fig. 1.4C). It was the intent of our experimental design to stimulate swimming to observe variation for the full range of potential directions. However, zebrafish larvae may vary elevation to a lesser degree under more natural conditions. For example, larvae respond to the flow generated by a predator's approach in the dark with a fast start (Stewart et al. 2014). When positioned ventral to the predator, larvae move downward at an angle of less than $30°$ and larvae positioned dorsal to the predator move with planar motion. Therefore the variation in elevation that we presently observed indicates the scope of possible 3D responses, rather than the directions that may occur in an encounter with a predator. Nonetheless, 3D escapes may be strategically beneficial for a prey (Domenici et al. 2011a). A trajectory that varies in elevation will be less predictable than planar motion and downward swimming has the

potential to offer refuge in the benthos. In addition, the locomotor system of a predator may be more capable of tracking prey with purely lateral motion.

Implications for motor control

The present results offer the opportunity to consider the motor control of elevation. Thinking about the directional control of the fast start has been greatly influenced by a model proposed by Foreman and Eaton, which focuses on the reticulospinal neurons that activate the motor neurons of the axial myomeres (Foreman and Eaton 1993). Based on experimental results in adult goldfish, the Mauthner neuron and two serial homologs activate the musculature for stage 1 on the side of the body contralateral to a stimulus. With a slight delay, stage 2 muscles are activated on the ipsilateral side with unidentified command neurons. According to Foreman and Eaton, variation in direction is generated by the differential sensitivity of the command neurons to the direction of a stimulus. A rostral stimulus is predicted to activate stage 1 neurons (i.e. the Mauthner and homologs) to maximally recruit contralateral musculature and thereby create a large yaw away from the stimulus. This change in heading would consequently be maintained by a relatively modest recruitment of the stage 2 neurons and associated ipsilateral muscles. In contrast, a caudal stimulus is predicted to generate a modest recruitment in stage 1 and a relatively large recruitment in stage 2 to direct swimming forward. Therefore, the fast start may be controlled to generate swimming in a full range of azimuth angles by varying the intensity and timing of activation in these pathways. We have currently observed that zebrafish larvae also direct their swimming at a variety of azimuth angles (Fig. 1.4B) and previous results have shown that the azimuth can be directed away from a present results. By taking advantage of the transparent bodies of these animals, calcium imaging served to establish the patterns of activity by the Mauthner neuron and its homologs.

In support of the model, all three of these neurons are activated by a rostral stimulus, but only the Mauthner neuron plays a role in response to a caudal stimulus (O'Malley et al. 1996). Experimental manipulations have shown that the fast start can be generated without the Mauthner neuron and its homologs with only subtle differences in kinematics (Kimmel et al. 1980, Liu and Fetcho 1999). Nonetheless, it is a reasonable inference that descending commands from the hindbrain serve to activate the contralateral and ipsilateral motor neurons that drive a fast start in a manner similar to that proposed by Foreman and Eaton. It follows that muscle activation that results from these commands would need to be modulated to permit control of elevation.

Recent work on the functional organization of motor circuits in zebrafish may help to explain the neuromuscular control of elevation. The myomeres that generate tail bending are innervated by separate pairs of primary motor neurons for the epaxial (dorsal to the horizontal septum) and hypaxial (ventral to the horizontal septum) regions (Westerfield et al. 1986, Menelaou and McLean 2012). The timing and intensity of the firing within the epaxial neurons may be varied independently from the hypaxial neurons (Bagnall and McLean 2014). Differential activation of these motor neurons is mediated by a spinal 'microcircuit' that alters motor neuron activation during swimming, which presumably alters muscular force. These differences in activation are stimulated by input from the vestibular system when zebrafish fail to maintain equilibrium. These microcircuits do not generate descending motor commands, but rather modulate the intensity of these commands during swimming, and this modulation can be sustained over multiple tail beats.

Fig. 1.9. Changes in elevation during a fast start. The results of our kinematic measurements support a model for the control of elevation in a fast start that is illustrated for a fast start that is directed downwards and towards the left side of the body. (A) Angular changes in the body are defined relative to its initial orientation, given by the orientation of the head (dashed gray line) and frontal plane of the body (in blue). (B) The elevation begins to adopt its course as the head changes pitch (in green) in stage 1, which continues in stages 2 (C) and 3 (not shown). Throughout these stages, the undulatory motion of the tail follows the downward course set by the head. (D) The temporal changes in yaw (blue curve) and pitch (green curve) are illustrated for the schematic motions shown above.
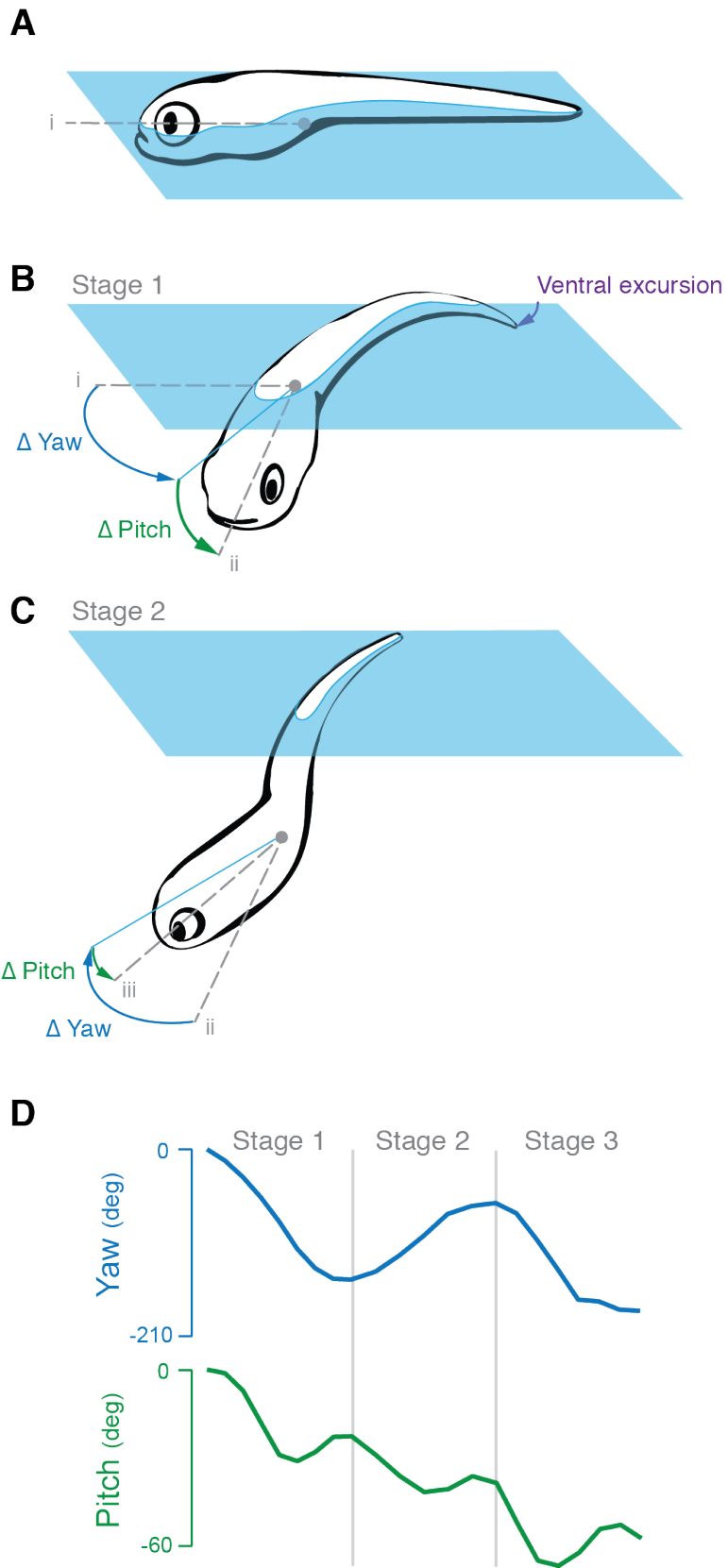
Our results are consistent with a role for spinal microcircuits in controlling the elevation of a fast start. For example, consider the events that occur when a larval fish executes a diving maneuver (Fig. 1.9). The pitching motion that directs swimming downwards could be generated by the hypaxial musculature generating greater force than the epaxial musculature along the length of the tail. Such would be the result of a microcircuit command that inhibited the primary motor neurons for the epaxial muscles while exciting the hypaxial muscles. This influence on the motor commands would span the stages of a fast start and explain how the pitching of the body is maintained throughout the maneuver (Fig. 1.9D). An advantage to this mechanism of control is that it allows for variation in elevation without hindering the speed of the fast start.

It is possible that elevation control may be applied to more than just larval zebrafish. The experimental designs of past studies have generally neglected a consideration of elevation. The fast start of freely swimming fish, which has mostly focused on adults, is commonly studied in shallow water or with video recordings of only a dorsal perspective. Fictive preparations for neurophysiology necessarily restrict body motion and have also neglected dorsoventral motion. Therefore, it remains possible that the fast start occurs in three dimensions among other species and stages of growth. The fast start may indeed be a more complex and evasive maneuver than previously appreciated.

CHAPTER 2: Sensation has a greater impact on predator evasion over locomotion

Introduction

An escape response allows prey to evade predators with fast locomotion (Bullock 1984). Because of its potential to directly affect survivorship, natural selection may favor animals that can execute an escape response with high locomotor performance. Indeed, the physiology and mechanics of locomotion features many traits that are likely adaptations for rapid motion. Escape responses are controlled by large-diameter command neurons (e.g. the giant axon of squid (Young 1938)), which often recruit specialized muscles (e.g. the axial musculature of fish (Eaton and Farley 1975)), which sometimes animate an appendage that function only during an escape (e.g. the uropods of crayfish (Johnson 1926)). Prey may direct this escape in an optimal direction (Weihs and Webb 1984), or may alternatively benefit from heading in an unpredictable (Humphries and Driver 1970) or variable (Howland 1974) direction. However, it does not necessarily follow that any improvement in speed or variation in heading will have a positive effect on survivorship. Fish predators commonly approach their prey at a relatively slow speed (Webb 1984, Higham 2007) and this could permit an escape by prey exhibiting speed and directionality that is sufficiently evasive, but well below physiologically-maximal performance. The aim of the present study was to test whether improvements in locomotor performance affect prey survival by examining predator-prey interactions in zebrafish.

We addressed this aim with a novel approach that combines experimentation with an application of pursuit-evasion modeling. Our methodology was developed to meet the challenges to understanding the coupled dynamics of predators and prey. This coupling emerges because motion by the prey may (or may not) be in response to the predator, which may (or may not) be a

response to prior motion by the prey. Regression analyses are generally insensitive to such interdependency, yet may succeed in resolving dominant features of successful prey (Walker et al. 2005) or predators (Wainwright et al. 2001). It is additionally helpful to study behavioral responses to an artificial predator or prey that is experimentally controlled and therefore not coupled (Wainwright et al. 2001) (Gabbiani 1999, Heuch et al. 1999, Wainwright et al. 2001, Shifferman and David 2004, Stewart et al. 2014). An alternative approach attempts to formulate a behavioral algorithm of one animal by considering their responses to the measured kinematics of the other. For example, this technique revealed that predatory bats track evasive moths by maintaining their heading, rather than attempting to anticipate the prey's direction (Ghose et al. 2006).

The present study also included measurements of predator-prey kinematics, but these provided a basis for modeling the behavior of both the predator and prey. Our model predicted the trajectories of both animals such that the probability of behavioral actions matched our observations when conducted over number simulations. This served as a probabilistic, agent-based model with the payout being the number of strikes that the prey survived before capture. The advantage of an experimentally validated model is that it allows for a predictive consideration of the effects of differences in behavior on prey survival. We performed our study on zebrafish (*Danio rerio*). The larval stage of this species serves as a model for studying the neurophysiological (Huang 2013, Bagnell and McLean 2014, Bianco and Engert 2015) and biomechanical (Müller, U. and van Leeuwen 2004, Li et al. 2016) basis of behavior. Predator-prey interactions may be experimentally replicated in the lab, where adults and juveniles strike at larvae with suction feeding and the larvae respond with a fast-start escape response (Stewart et al. 2013). These are the two principle behaviors that characterize a broad diversity of piscivorous

interactions (Weihs and Webb 1984, Walker et al. 2005). When approaching an evasive prey, zebrafish predators approach much more slowly than their maximum speed (Stewart et al. 2013), which is common among suction-feeding fishes (Webb 1984, Higham 2007). A slow approach presumably allows greater control over the direction and timing of the suction feeding, which is limited to a brief duration over a small region in front of the mouth (Holzman et al. 2008, Holzman and Wainwright 2009). The prey, by contrast, responds with an explosive escape response with speed that exceeds that of the predator. As suggested by prior experiments (Fuiman 1994) and pursuit-evasion models (Weihs and Webb 1984), the relative speed of predator and prey greatly determines strategy. We, therefore, performed experiments with juvenile and adult predators with a nearly two-fold difference in body length.

Material and Methods

Animal Husbandry

All experiments were conducted on zebrafish (*Danio rerio*, Hamilton 1822) with larvae (5 - 7 days post fertilization, dpf) that were preyed upon by older fish of the same species. To examine how these interactions vary with the size of the predator, we performed one set of experiments using adults ($\geq$ 9 months old, Mean $\pm$ 1 SD = 3.4 $\pm$ 0.5 cm, n = 19) and another using juvenile predators (3 - 4 months old, 2.0 $\pm$ 0.4 cm, n = 19). All fish were bred from wild-type (AB line) colonies housed in a flow-through tank system (Aquatic Habitats, Apopka, FL, USA) that was maintained at 28.5 $^{\circ}$C on a 14:10 h light:dark cycle. To produce larvae, the fertilized eggs from randomized mating were cultured according to standard techniques (Westerfield 1993) Predators were motivated to feed by fasting for a period of 7 - 14 days prior to an experiment.

Kinematics

We arranged the lights and cameras for high-speed recordings of both fish with high-contrast images. A hemispherical aquarium (⌀ = 8.5 cm) was composed of white acrylic, which served as a translucent diffuser of the IR illumination (940 nm) provided by three lamps (CM-IR200-940, CMVision, Houston, TX, USA), positioned below (Fig. 2.1A). These lamps provided high-intensity illumination that was invisible to the fish (Robinson et al. 1993), while visible illumination at low intensity was provided by overhead fluorescent lights. Each camera (FASTCAM Mini UX50, Precision Photron Inc., San Diego, CA, USA) was fitted with a 55 mm lens (f/2.8 Micro Nikkon AIS, Nikon Inc., Melville, NY, USA) and positioned at a distance that permitted a view of the entire aquarium. The cameras were angled above the aquarium to allow both fish to be viewed by at least two cameras when the fish were positioned close together. The cameras were synchronized to record at a 1,000 fps (at 1024 x 1024 pixels) with a common TTL trigger and controlled with the manufacturer's software (PhotronFASTCAM Viewer).

Predation experiments were performed by recording the swimming of one predator and one prey fish in the aquarium (Fig. 2.1A). This began by placing the fish on opposite sides of a partition. Following a 15 min acclimation period, we lifted the partition and observed the fish until the predator successfully ingested the prey. Using an end-trigger to the high-speed cameras, we saved recordings from ~0.5 s before the first predatory strike and until ~0.5 s after the prey was captured.

Our video recordings were used to perform measurements of 3D kinematics. We calibrated the cameras by recording a static body that we constructed with 48 landmarks of known relative position, which was placed in the center of the aquarium.
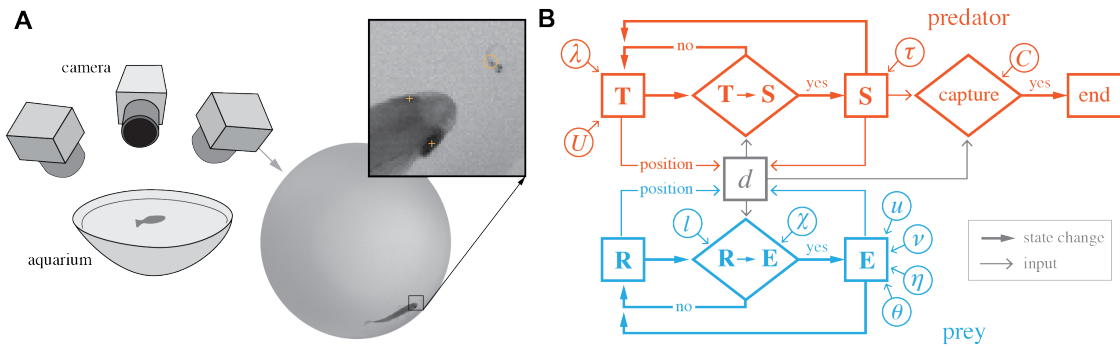
Fig. 2.1. Kinematic measurements and probabilistic, agent-based modeling for studying predator-prey interactions in zebrafish. (A) Three high-speed video cameras recorded video of one larval prey and one predator fish (adult or juvenile) that were placed in a hemispherical aquarium. A representative video frame (cropped to the margin of the aquarium) shows an adult in close proximity to the prey. In the inset, orange markers denote the locations of morphological landmarks used to describe the position of the two fish. This consisted of the position of the two eyes for the predator ("+") and the posterior margin of the swim bladder in the prey (open circle). (B) A flow chart illustrates the major components of the model used to simulate the interactions between predators and prey (see Table 2.1 for symbol definitions and parameter values). Each fish behaves according to an algorithm is specific to a particular behavioral state and the probability of transitioning between states is determined by random-number generators with probability distributions matching kinematic measurements (Fig 2.2). Predators (in red) operate between Tracking (T) and Striking (S) states and prey are either Resting (R) or Escaping (E). The outcome of a strike is determined by the capture probability (*C*, Eqn. 2.2). See Materials and methods for details.

A direct-linear transform (DLT) was calculated using 'Digitizing Tools' software in MATLAB (2015a, MathWorks, Natick, MA, USA) (Hedrick 2008) from manually selected coordinates of these landmarks from the perspective of the three cameras. Using a custom script in MATLAB, we found the body positions of predator and prey fish by selecting landmarks from two camera views and using the DLT to determine the coordinates in 3D space. We used the position of the predator's two eyes to calculate a mean position that approximated the buccal cavity (Fig. 2.1A). The posterior margin of the swim bladder was found on the prey's body, which approximates the center of mass (Stewart et al. 2010). The initial heading of the prey was approximated by matching an ellipsoid (using the 'regionprops' function in MATLAB) to the body of the prey and measuring the angle of the major axis of the ellipsoid. All subsequent heading measurements of the prey was defined as the average angular displacement of prey during an escape and was relative to the prior heading of the prey. We acquired the landmark positions at four key events in each interaction between predator and prey: at (1) the initiation of a predator's approach toward the prey, (2) the middle time point of the duration of suction feeding by the predator and the (3) initiation and (4) completion of the prey's escape response.

Descriptive Statistics

Descriptive statistics were used to characterize the probability of actions by the predator and prey during predation experiments. We recorded the predator-specific parameters of the strike distance (s), the distance from the prey at which a strike (i.e. a suction feeding event) was initiated, and the strike duration (τ), which was defined as the period between the opening and closing of the mouth during suction feeding. For the prey, we found the reaction distance (l), the distance from the predator at which the escape response was initiated. The prey's kinematics were additionally characterized by the escape angle (θ), the angular change in heading from the

resting orientation to the escape path. The escape duration (η) included the period for all stages of the C-start and subsequent undulatory swimming, until the larva ceased moving. The frequency distribution for each of these parameters was found to be well approximated by the following lognormal probability density function:

$$f(x) = \frac{1}{x\sigma\sqrt{2\pi}} e^{\left[-\frac{(\ln(x)-\mu)^2}{2\sigma^2}\right]}, \qquad (2.1)$$

where x is a particular behavioral parameter (s, τ, l, θ; or η), μ is the log mean, and σ is the log standard deviation. We determined best-fit values for μ and σ for each behavioral parameter by maximum-likelihood (the 'fitdist' function in MATLAB). Instances where the predator captured the prey, parameters for the prey were not included in the dataset.

The probability that the strike of a zebrafish predator is successful depends critically on the distance between the mouth of the predator and the prey (Stewart et al. 2013). Strikes were therefore measured as a function of distance. We binned our distance data using a fixed number of bins and calculated the ratio of number of observations in the bin over the total sample size (Fig. 2.2F). These binned measurements revealed that the probability of a successful capture (C) was well characterized by the following sigmoidal function:

$$C(d) = \left[1 + e^{-r(d-d_0)}\right]^{-1}, \qquad (2.2)$$

where d is the distance between predator and prey, d_0 is the decay distance, and r is the decay rate. The best-fit values for d_0 and r were determined by least squares (using the 'sqcurvefit' function in MATLAB).

All parameters for the prey and predators were compared between experiments with adult predators and juvenile predators. Because these measurements failed to conform to normal distributions, we performed statistical comparisons using non-parametric statistics. In particular, we used the two-sample Kolmogorov-Smirnov test (i.e. KS-test) (Massey 1951), which does not

assume any particular distribution for the data.

Probabilistic, agent-based model

A probabilistic, agent-based model was developed to simulate the conditions of our experiments. This model predicted the 2D motion of a predator and prey (Isaacs 1965) according to algorithms that were specific to the behavioral state of each of these agents (Fig. 2.1B). The predator's states were Tracking and Striking and the prey's were Resting and Escaping. The duration of states, probability of transitioning between states, and probability of prey capture were determined by random-number generation that conformed to the probability distributions and range of values that we measured. Therefore, the model treated the predator and prey's actions as probabilistic, but each outcome of an interaction also depended on the determinism of the kinematics of the two agents. Simulations were scripted in MATLAB to calculate the motion of both agents and their behavioral states, which consequently determined the number of unsuccessful strikes before prey capture.

Each simulation began with the predator in the Tracking state, where it moved at an approach speed with a direction that was always headed toward the prey, with perfect information about the prey's position (Fig. 2.1B). If the prey was motionless, then the solver would advance in time to the strike or escape initiation, whichever was found to occur first. Otherwise, the solver would resolve both predator and prey motion with a fixed time step of 5 ms. In this regime, the predator adjusted its heading to track the prey with a temporal time delay, λ. The predator's transition into the Striking state occurred when the prey was within a particular value for the strike distance. This value was determined a-priori by the generation of a random value (using the 'random' function in MATLAB) according to the lognormal probability density function (Eqn. 2.1) for measured values of strike distance. The capture probability, C, for a

particular strike depended on the distance between the agents in the middle of a strike, according

to our measured parameter values for this relationship (Eqn. 2.2). The simulation was terminated

if a strike was successful; otherwise the predator reverted to the Tracking state after completion

of the strike duration (Fig. 2.1B). The value of strike duration was determined by the generation

of a random value from the lognormal probability density function from measured values. Single

values for the predator speed and delay were used for all simulations (Table 2.1) and were

determined by trial-and-error to replicate the distribution of the measured number of

unsuccessful strikes before prey capture. These values were found to approximate measurements

reported in prior studies (Stewart et al. 2013, McHenry and Lauder 2005). The model

simultaneously determined the actions of prey (Fig. 2.1B). Prey behavior was modeled with

Resting and Escaping states because larval zebrafish generally remain still between periods of

rapid swimming initiated by an escape response (Stewart et al. 2013, Stewart et al. 2014). The

prey began each simulation in the Resting state, where it was motionless and positioned at a

random distance from the predator that was within the aquarium diameter ($\oslash$ = 8.5 cm). The

prey transitioned into the Escaping state when the predator moved within the reaction distance,

after a latency (Nair et al. 2015). During an escape, the speed of prey varied as a single saw-

toothed pulse, with the maximum value (the peak of the sawtooth) attained at 0.2η, where η is the

escape duration. We found that this function well-characterized prey speed using a frame-by-

frame kinematic analysis of escape swimming for 12 larvae. The amplitude of the saw-toothed

pulse represented the maximum escape speed, u, observed in our 12 recordings. During the

escape, the prey was assumed to follow a straight path in a direction determined by the escape

angle and escape direction.

Table 2.1. Behavioral parameters and probability distributions

Variable	State	Adult predator	Juvenile predator
Predator			
Approach speed, U (m s^{-1})	T	$U = 0.13$	$U = 0.05$
Predator delay, λ (ms)	T	$\lambda = 10$	$\lambda = 10$
Strike distance, s (m)	T $\rightarrow$ S	$\mu_d = -4.980, \sigma_d = 0.448$ ($N = 51$)	$\mu_d = -5.100, \sigma_d = 0.648$ ($N = 103$)
Strike duration, τ (s)	S	$\mu_\tau = -3.166, \sigma_\tau = 0.331$ ($N = 53$)	$\mu_\tau = -3.208, \sigma_\tau = 0.399$ ($N = 54$)
Capture probability, C	S	$r = -0.573, d_0 = 5.20$ ($N = 77$)	$r = 1.99, d_0 = 1.60$ ($N = 91$)
Prey			
Reaction distance, l (m)	R $\rightarrow$ E	$\mu_l = -4.546, \sigma_l = 0.587$ ($N = 73$)	$\mu_l = -4.941, \sigma_l = 0.582$ ($N = 91$)
Escape angle, θ (rad)	E	$\mu_\theta = 0.144, \sigma_\theta = 0.449$ ($N = 206$)	$\mu_\theta = 0.144, \sigma_\theta = 0.449$ ($N = 206$)
Escape duration, η (s)	E	$\mu_\eta = -1.369, \sigma_\eta = 0.552$ ($N = 62$)	$\mu_\eta = -1.167, \sigma_\eta = 0.5234$ ($N = 91$)
Escape direction, υ	E	$\upsilon = 0.696$ ($N = 206$)	$\upsilon = 0.696$ ($N = 206$)
Escape latency, χ (ms)	E	$\chi = 8$ ($N = 15$)	$\chi = 8$ ($N = 15$)
Escape speed, u (m s^{-1})	E	$u = 0.4$ ($N = 12$)	$u = 0.4$ ($N = 12$)

T, Tracking; S, Striking; R, Resting; E, Escaping; μ, log mean; σ, log standard deviation; r, decay rate (mm^{-1}); d_0, decay distance (mm).

The reaction distance, escape angle, and escape duration were determined by random numbers with probability density functions matching experimental measurements. The escape angle was defined with respect to the prey's frame of reference, with $\theta = 0°$ corresponding to and axis defined by forward motion. This angle was directed with respect to the right or left side of the body by the escape direction. The escape direction was defined as the probability that the escape angle was directed toward the side of the body facing away from the predator, with a value (Table 2.1) that was previously measured (Stewart et al. 2013).

This model simplified many aspects of the complexity of predator-prey interactions. It assumed that the kinematics of the two fish may be approximated with two-dimensional motion that is not bounded by an aquarium. Simulations were halted if prey successfully escaped on 20 occasions, which reflected the observed maximum and guarded against an errant simulation of infinite duration. The model's use of random number generation considered the probabilistic effects of biomechanics and neurophysiology without explicitly articulating those elements. For example, capture success was treated as a distance-specific probability (Eqn. 2.2) that modeled neither the effects of a predator's suction-feeding hydrodynamics, nor the propulsive forces generated by an escaping prey. The number of successful escapes before capture for all experiments was compared to the same metric for 1,000 simulations. This comparison was executed by a two-sample Kolmogorov-Smirnov test, which was chosen over a Kruskal-Wallis test because of its emphasis on the shape of the distribution.

We designed a parameter analysis to evaluate the parameters that had the greatest effect on prey survival. This was achieved by running Monte Carlo simulations of the model for a 1,000 simulations where one parameter was varied between -90% and 100% of their original mean values at increments of 10%. For parameters described by a probability distribution, the

log-mean parameter, μ, was adjusted to create the desired percent-change in the mean of the distribution, while σ was held constant. The range of possible random values for each distribution was also adjusted to retain the same cumulative probability range in the probability distribution. Each parameter variation yielded 1,000 trials, each where the prey has escaped a varying amount of times. The effect of these manipulations was assessed by comparing the measured number of escapes the prey made against the model's prediction without any parameter variation (% change = 0) using a Kruskal-Wallis test. The results for these comparisons are displayed as escape probabilities in the main text, though the number of escapes plots can be viewed in the supplements (Fig. S2.2).

Results

Kinematics

The behavior of both predator and prey were similar whether the predators were juvenile or adult zebrafish. Prey responded similarly, having indistinguishable differences in escape angle (KS-test: $P = 0.86$, $n = 164$) and with modest, though significant, differences in reaction distance (KS-test: $P < 0.001$; $n = 164$) and escape duration (KS-test: $P = 0.04$, $n = 153$) (Fig. 2.2B - C). For example, prey reacted at a mean distance to juvenile predators ($\bar{l} = 0.84$ cm, $n = 91$), which was about two-thirds the reaction distance to adults ($\bar{l} = 1.26$ cm, $n = 73$). Escape swimming lasted for about one-third of a second, with the response to juveniles ($\bar{\eta} = 0.35$ s, $n = 91$) being only 50 ms longer than to adults ($\bar{\eta} = 0.30$ s, $n = 62$). Prey escaped earlier to adult predators (KS-test: $P = 0.02$, $n = 89$) by 41 ms, on average, relative to the mid-duration of suction feeding.

prey parameters

predator parameters
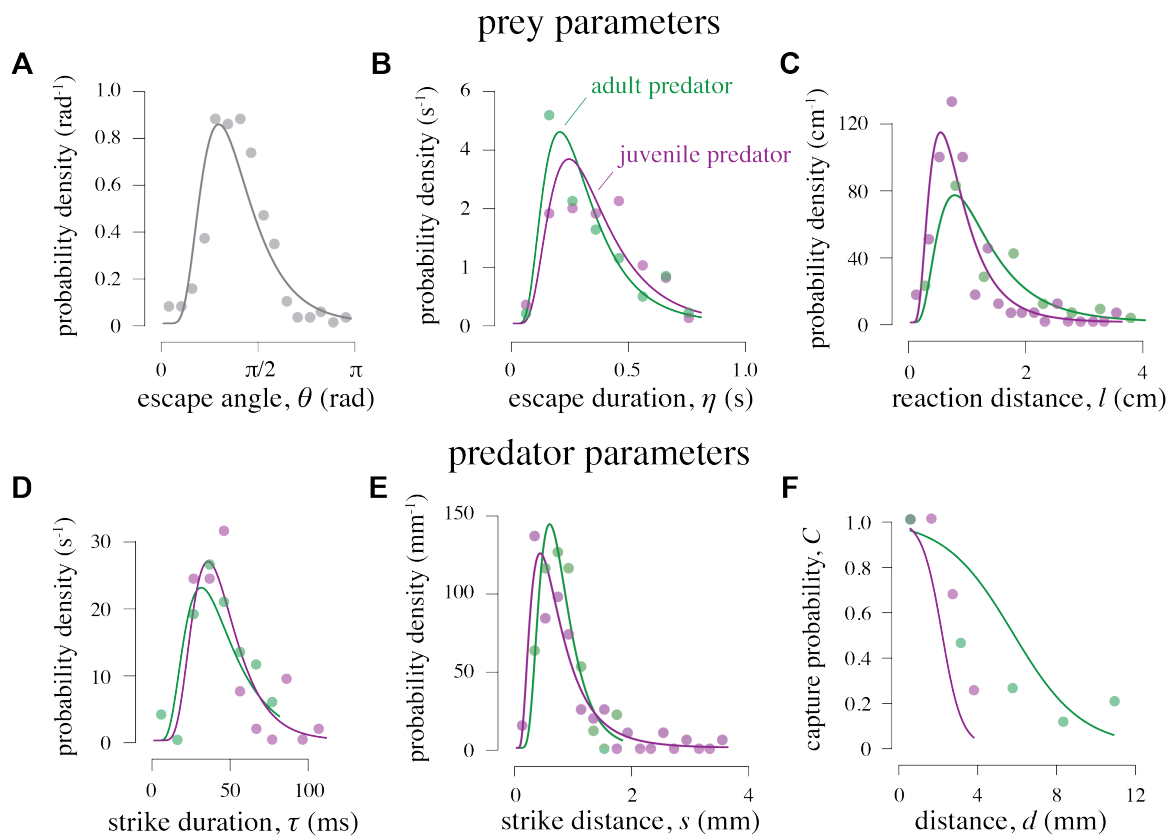
Fig. 2.2. Descriptive statistics of swimming kinematics. (A - E) The probability measurements (circles) and probability density function (Eqn. 2.1) fits for experiments where the predator was a juvenile (purple) or adult (green) predator. Parameters were measured from the kinematics of prey (A - C) and predators (D - E) (See Table 2.1 for sample sizes). Points on graph denote measured probability density. Each point represents a bin of the respective data and the size of the bins was determined using the Freedman-Diaconis rule. The value of each bin is the probability density and is calculated as the ratio of the number of observed samples of data in the bin over the product of the total sample size and the bin width. The curves represent the continuous, least squares fit to the discrete data. (F) The capture probability was examined as it varies with distance between the predator and prey (Eqn. 2.2).

Juvenile and adult predators were not significantly different in either their strike distance (KS-test: $P = 0.08$, $\bar{\eta} = 7.6$mm, $n = 154$), or strike duration (KS-test: $P = 0.87$; $\bar{\tau} = 44$ ms, $n = 107$) (Fig. 2.2D - E). Therefore, much of the behavior of predator and prey were similar, despite the fact that the adults were nearly twice the body length of the juveniles.

Despite having similar behavior, adult and juvenile predators differed in capture performance. Juveniles did not succeed in capturing prey beyond a distance of 3.2 mm ($n = 91$), whereas adults captured prey at a maximum distance that was about 3-times greater (10.4 mm, $n = 77$). In the relationship between capture probability and distance (Eqn. 2.2), the decay distance was used to indicate the spatial range of high capture probability. By this metric, the strike of adult predators also exhibited a range that was slightly greater than 3-times the distance of juveniles (Table 2.1, Fig. 2.2F). We tested whether this result was due to juveniles approaching the prey with inferior accuracy by measuring the bearing angle of predators. This angle corresponds to the radial position of the prey relative to the predator's heading, such that a predator is perfectly accurate for a prey position of 0°. The bearing angle when they prey initiated an escape was not significantly different (KS-test: $P = 0.15$) between juveniles ($n = 91$) or adults ($n = 77$). However, bearing angles changed such that there was a significant difference (KS-test: $P = 0.008$) between adults and juveniles when measured at the moment of mid-gape. In particular, adult predators succeeded in achieving a median bearing of 131° (Mean $= 35.3^{\circ}$), whereas the same metric was 30.0° (Mean $= 39.2^{\circ}$) in juveniles. This suggests that adults were more accurate in their strikes and more effectively adjusted their heading in the time between escape and strike.
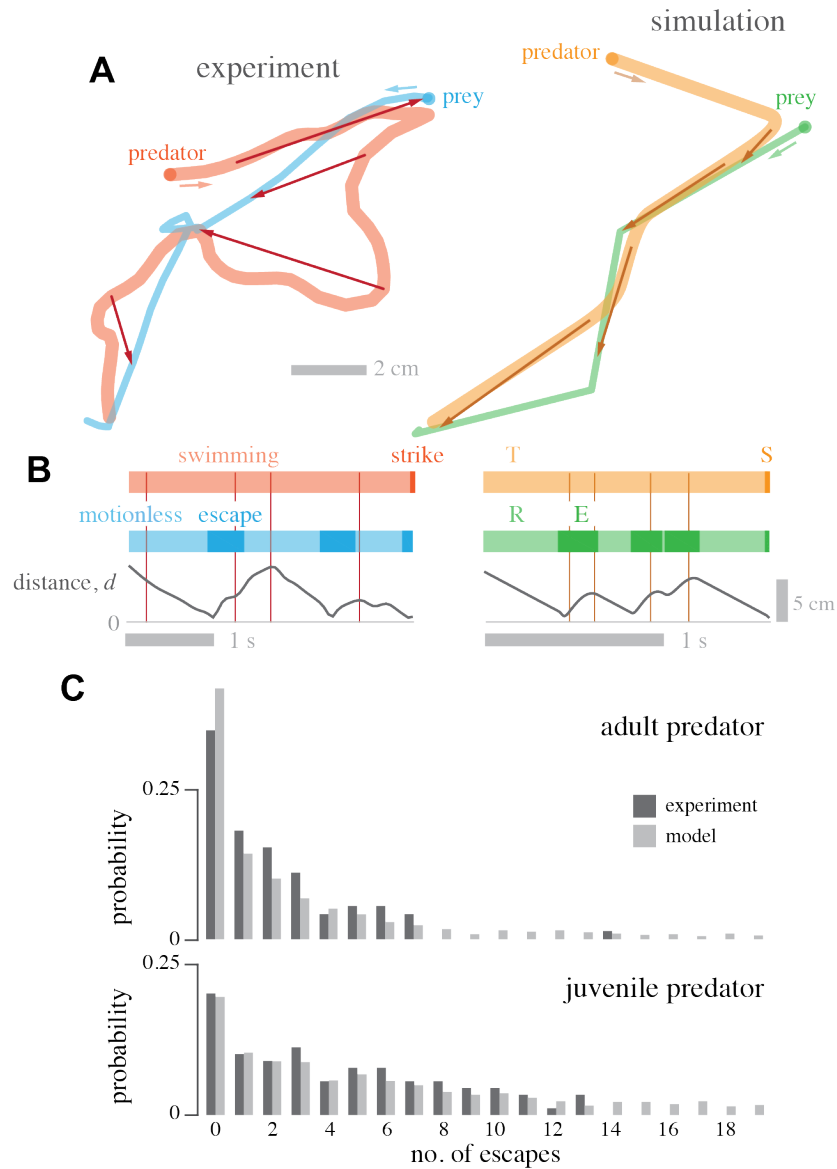
Fig. 2.3. Comparison between experimental measurements and modeling. (A) Trajectories of predator and prey from a representative experiment (left) and simulation (right). The position of predator and prey that correspond to particular time points are shown with connecting arrows. (B) Ethograms for these trajectories illustrate the temporal changes in the predator's swimming and strike (left), which are respectively modeled by the Tracking (T) and Striking (S) (Fig. 2.1B) states (right). The prey's behavior while motionless and during escape (left) were respectively modeled as Resting (E) and Escape (E) modes (right). For both ethograms, the distance (d) between predator and prey are shown. Particular moments in the trajectories are highlighted with vertical lines that correspond with the same-colored arrows in (A). (C) The probability that a prey survives over a particular number of strikes is shown adult (above) and juvenile (below) predators for experiments (dark gray) and simulations (light gray).

Probabilistic, agent-based model

The trajectories of predator and prey fish followed paths that were qualitatively similar to that predicted by our pursuit-evasion model. For most of the duration of our experiments, predators were observed to be swimming toward the prey (Fig. 2.3A). In contrast, the prey was generally motionless, except when executing escape swimming. The predators and prey followed a more circuitous path in the predation experiments than the motion prescribed by our model (Fig. 2.3B). Nevertheless, the temporal sequence of events in the model offered a reasonable approximation of the kinematics of live predator-prey interactions.

The model accurately predicted the broad quantitative patterns of our experimental results. This was assessed by the probability of the prey surviving over a particular number of strikes. In our experiments, prey exhibited the greatest probability of being captured on the first strike with monotonically decreasing probabilities over subsequent strikes (Fig. 2.3C). Adults were more successful on the first, second and third strikes than juveniles, which consequently exhibited a more even probability distribution. The model was successful in replicating these trends, which were found to be statistically indistinguishable for both adult (KS-test: $P = 0.93$, $n = 73$) and juvenile (KS-test: $P = 0.86$, $n = 91$) predators. Furthermore, all trends from the parameter analyses of the pursuit-evasion model were similar between the adult (Fig. 2.4) and juvenile (Fig. S2.1) predators.

A parameter analysis of prey parameters revealed that escape speed and reaction distance were the only parameters with a substantial effect on prey survival. This result was determined by adjusting the probability distribution of each parameter to generate a percent change in the mean value of that parameter among 1,000 simulations.
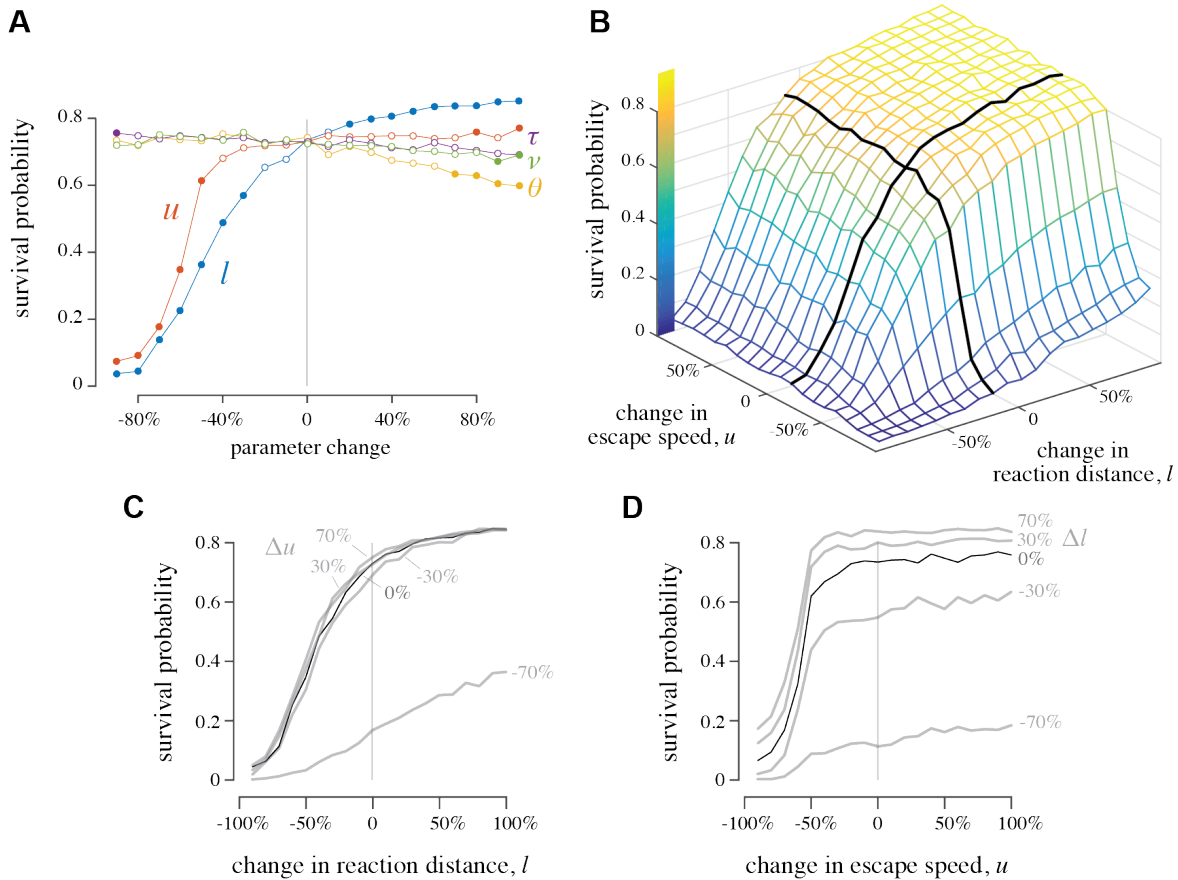
Fig. 2.4. Parameter analysis of the probabilistic, agent-based model to examine the effects of parameters on escape probability. (A) We individually varied the mean parameter value among simulations by manipulating the distribution (Fig. 2.2) of our measurements (see Table 2.1 for parameter definitions and values). Each point represents the survival probability of prey among 1,000 simulations and filled circles denote a significant difference (KS-test: $P < 0.05$) from the observed probability. Simulations that varied in escape angle (θ) differed by an interval of 0.127 rad. (B) Variation in escape probability was examined with respect to both escape speed and reaction distance. The same simulation results are shown with respect to changes in escape speed (C) and reaction distance (D). All simulations used an adult predator, although similar results were obtained with a juvenile predator (Fig. S2.1).

Generating these changes in escape duration, escape direction, and escape angle led to statistically insignificant or small changes in escape probability (Fig. 2.4A). An increase in escape speed similarly had a negligible effect on survival, but survival probability did decline when speed was reduced by 50% or more. However, survival was most sensitive to reaction distance. Increases to the mean reaction distance caused escape probability to increase up to 16% and decreases in the mean reaction distance by 30% or more had a dramatic adverse effect on survival (Fig. 2.4A).

We examined how the effect of reaction distance varies with escape speed by conducting a two-dimensional parameter analysis (Fig. 2.4B). It was not until speed was reduced by more than 50% that the relationship between response distance and survivor was altered. For example, reducing speed by 70% yielded a distinct curve, the shape of which was similar to the sigmoid generated at higher speeds (Fig. 2.4C). Alterations in response distance did affect the relationship between escape speed and survival, though the shape of this curve was largely unaltered (Fig. 2.4D). This suggests little evidence for an interactive effect on survival between escape speed and response distance.

Discussion

We found that the survival of larval fish does not increase by escaping at a faster speed or by varying direction, but only by responding from a greater distance. These results were attained through a parameter analysis of a model (Fig. 2.1B) that calculated the trajectories of predator and prey and the outcome of predatory strikes (Fig. 2.3A - B). This probabilistic, agent-based model successfully replicated the broad patterns of survival (Fig. 2.3C) by simulating behavioral actions that matched our measurements (Fig. 2.2). Our analysis of its predictions suggests that

54

prey survival in fishes may be enhanced by increasing the performance of sensing and not locomotion.

Locomotor performance and prey survival

The survival of prey depends largely on the actions of the predator. In contrast to the explosive speed of an escape response (Müller and van Leeuwen 2004), zebrafish predators tend to approach their prey substantially slower than their capacity, often by braking (McHenry and Lauder 2005). The approach speed amounted to less than one-third the maximum speed of escaping larvae (Table 2.1), which is consistent with previous measurements (Stewart et al. 2013). The approach speed relates strategically to the mechanics of feeding. The suction feeding of fishes succeeds in capturing prey in only a small region around the mouth over a duration of merely tens of milliseconds (Ferry-Graham 2003, Higham 2005, Holzman et al. 2007). A slow approach is common among suction feeding fishes and is likely a means of enhancing strike accuracy (Webb 1984, Higham 2007). This style of predation is seen over many species of fish (Higham et al. 2007). Furthermore, our data suggest that zebrafish predators are more likely to capture predator when approaching larval zebrafish with slower approach speeds (Fig. S2.3). Therefore, the limited range of suction feeding may constrain some predators to a slow approach while offering prey an opportunity to escape (Holzman and Wainwright 2009). Despite this strategic advantage for prey, adult zebrafish captured prey on the first strike more than one-quarter of the time and rarely needed more than three strikes to be successful (Fig. 2.3C).

The effectiveness of an escape has previously been considered by classic pursuit-evasion models of fish predation. Classic models resolve how the direction of an escape affects the distance between predator and prey with analytical mathematics (Isaacs 1965, Weihs and Webb 1984). They generally model a single encounter and assume that both animals move with a fixed

heading and speed over time. A recently developed version predicted that animals like zebrafish operate in a 'slow-predator' domain, where the predator moves more slowly than the prey (Soto et al. 2015). In this domain, no optimal escape angle exists and prey may rather evade predators with a broad range of escape directions and this range is only modestly expanded by a faster escape. In contrast, the predator gains a strategic advantage when the approach at a faster speed than the prey's escape (Weihs and Webb 1984). Consistent with these ideas, we found a monotonic decrease in survival as we reduced escape speed below half of the observed value (Fig. 2.4A) in our simulations. In addition, we found only modest differences in survival between experiments using adult and juvenile predators (Figs. 2.2, 2.3C), despite a nearly two-fold difference in body size. This would also be expected by classic theory because the interactions operate in the slow-predator domain in both cases. It follows from this theory that prey strategy benefits greatly by escaping faster than the predator, but further increases in speed offer diminishing returns.

Granted, in the 'fast-predator' domain, it could be postulated that there could be profound differences in the results from our model. Studies have shown that the kinematics of an escape response matter greatly when escaping predators (Howland 1974, Domenici 2001). For example, in classical pursuit-evasion models, the escape angle is a critical parameter for survival (Weihs and Webb 1984). Furthermore in situations when the predator is faster than the prey, prey adapt other behaviors, such as shoaling, as a predator defense (Pitcher 1986). However, these studies do no consider the effect of sensation can have on prey survival. Currently, our model cannot address this domain of predator-prey interactions. However, future studies with the presented model could examine how important the kinematics of escape are relative to sensation.

The strategic conditions exemplified by zebrafish have the potential to be applicable to a

diversity of fish species, but represent a special case among predator-prey interactions. Suction feeding is ubiquitous among fishes and a slow approach is common (Webb 1984, Higham 2007). However, not all fish predators are slower than the prey. Ram-feeding fishes strike at prey while swimming at a relatively high speed and may thereby place prey at a strategic disadvantage. Success in ram feeding may, in-turn, require superior coordination in directing and timing a strike (Wainwright 2001). Ram feeding therefore shows greater similarly in strategy to flying predators such as birds (Shifferman and David 2004), bats (Ghose et al. 2006), and insects (Combes et al. 2012). In these systems, the escape direction emerges as an important factor in prey strategy (Domenici et al. 2011a, Domenici et al. 2011b). This direction may conform to an optimal value (Weihs and Webb 1984), or may benefit prey by being unpredictable (Humphries and Driver 1970). Other factors, such as the turning radius of an escape trajectory (Howland 1974), or the rate of changes in direction (Humphries and Driver 1970) additionally become important when the predator is faster than the prey.

Prey survival depends on reaction distance

The reaction distance has broad strategic significance. The predictions of pursuit-evasion models support the simple notion that prey are more evasive if they start from further away (Isaacs 1965, Weihs and Webb 1984, Soto et al. 2015). This principle is consistent with evolutionary models that contrast the fitness benefit of responding from a distance against its potential costs (Ydenberg and Dill 1986, Cooper and Blumstein 2015). For example, escape responses that are initiated at high frequency may be energetically expensive, prohibit foraging, or succeed in revealing cryptic prey (Broom and Ruxton 2005). Responding from a great distance may even be inferior on purely strategic grounds. A prey that is slower than a predator, but capable of executing a tight turn, may benefit from initiating this maneuver at the final moments of a

predatory strike (Howland 1974). Therefore, a greater response distance offers a clear strategic benefit in zebrafish (Fig. 2.4), but may not be universally advantageous.

The primacy of reaction distance underscores the strategic importance of predator detection. Fish sense water flow with the mechanosensory lateral line system and this sensory modality is necessary for zebrafish larvae to survive predation (Stewart et al. 2013). The bow wave of flow generated ahead of a gliding predator succeeds in triggering a fast start in zebrafish larvae within a distance of 1.3 cm (Stewart et al. 2014), which is a range that includes many of the responses that we recorded (Fig. 2.2C). Although flow-mediated responses permit a close approach by the predator, the response is rapid and may trigger an escape in less than 10 ms (Liu and Fetcho 1999). Escape responses may also be elicited by a looming visual stimulus (Bianco et al. 2011), but the demands for visual processing necessitate a latency of at least 200 ms (Burguess and Granato 2007). Nonetheless, the greatest reaction distances that we observed were likely generated by the visual appearance of the predator. Therefore, the visual system offers prey fish the means to enhance survival by responding to a predatory threat from a distance (Fig. 4). Vision and flow sensing may be augmented by olfactory cues (Waldman 1982), though zebrafish do not acquire a sensitivity to the alarm pheromone Schreckstoff until a later stage of growth (> 48 dpf).

Summary

We found that zebrafish larvae operate in a slow-predator strategic domain when preyed upon by adults and juveniles of the same species. As a consequence, increasing the speed or varying the direction of an escape response shows a negligible effect on survival (Fig. 2.4). Survival may instead be enhanced by initiating the escape from greater distance by rapidly identifying the predator as a threatening visual stimulus. These findings offer valuable insight into the key

strategic factors that govern predator-prey interactions in a diversity of fishes and other animals that operate with a similar strategy.
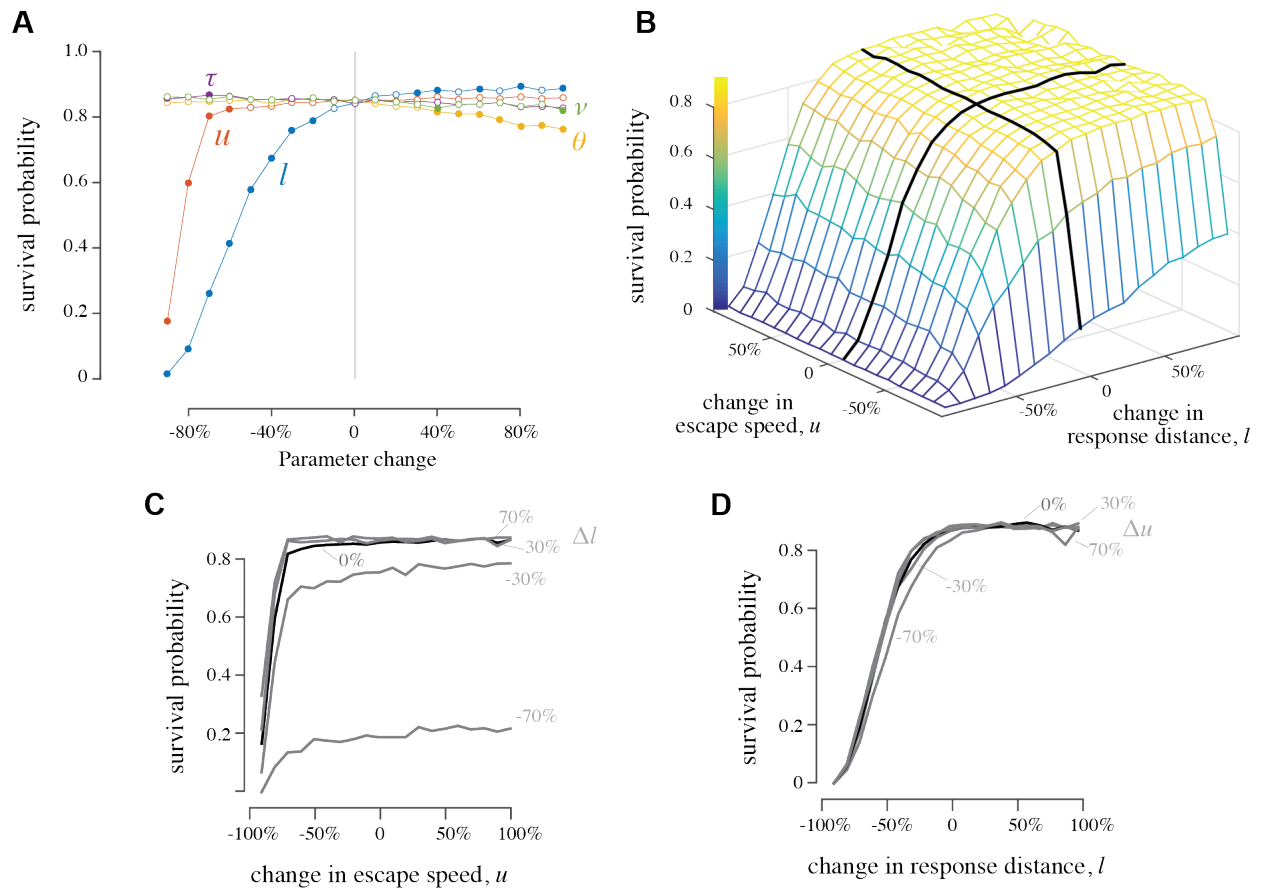
Fig. S2.1. Sensitivity analysis of the probabilistic, agent-based model with a juvenile predator. (A) We varied the mean of the distribution for each prey parameter by manipulating the log-mean value (see Table 2.1 for parameter definitions and values), with each point representing the result of 1,000 simulations. Solid points represent significant differences (KS-test: $P < 0.05$) from a 0% change. (B) Variation in escape probability was examined with respect to both escape speed and reaction distance. The same simulation results are shown with respect to changes in escape speed (C) and reaction distance (D).
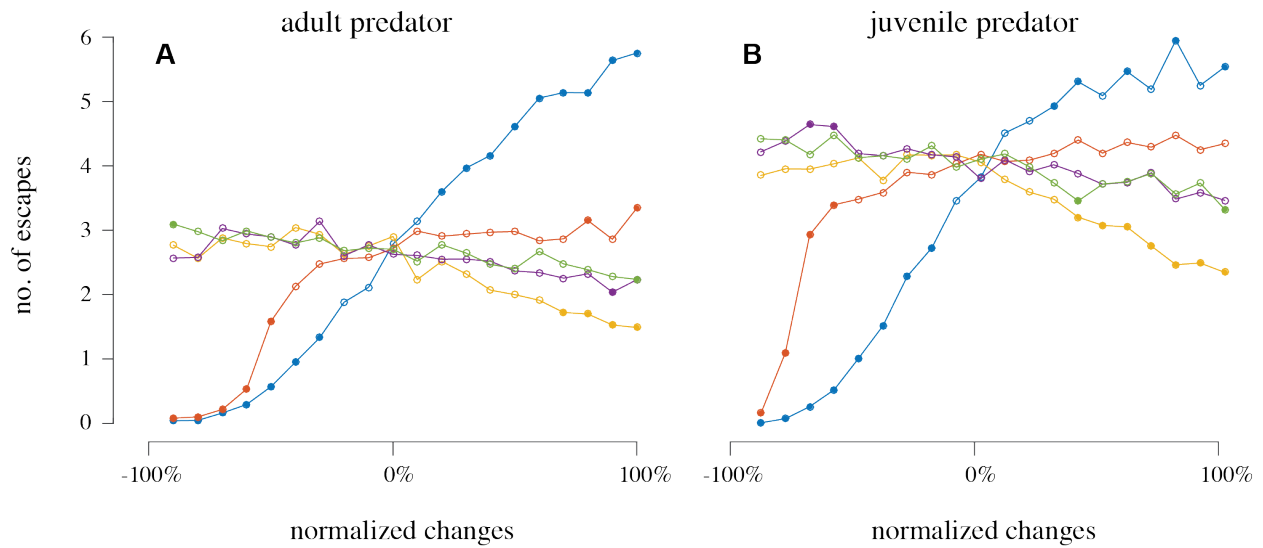
Fig. S2.2. The number of escapes prior to capture generated by the sensitivity analysis of the probabilistic, agent-based model. These are the sample simulations from which survival probability was determined with respect to differences in parameter values for (A) juvenile predators (same simulations as in Fig. S2.1A) and (B) adult (same simulations as in Fig. 2.4A). The shapes of these curves are different from when they are presented as survival probability because a probability cannot exceed a value of unity.

CHAPTER 3: Larval fish escape strategy is both optimal and unpredictable

Predation plays a critical role in the population dynamics, trophic interactions, and individual fitness of a broad diversity of species. Despite this importance, it is unknown what escape strategies prey employ to evade a predator's strike. Classic behavioral and theoretical studies suggest that, barring any constraints or bias toward a refuge, two major strategies serve to enhance prey survival. The protean strategy (Humphries and Driver 1970) favors high variability in the escape direction to challenge a predator's ability to anticipate a prey's heading. Alternatively, prey employing an optimal strategy are predicted to control their escape in the direction that maximizes their distance from a predator (Weihs and Webb 1984). With few exceptions (Corcoran and Conner 2016), investigators have not tested the predictions of strategic models against measurements of the kinematics of the escape. As a consequence, it is generally unclear how survival is determined by the sensing and locomotion of prey. The present study aimed to test the strategy of the escape response used by larval zebrafish (*Danio rerio*), which is a model for understanding the neurophysiological and biomechanical basis of locomotion (Liu and Fetcho 1999, Dunn et al. 2016, Koyama et al. 2016).

The escape response is an explosively fast maneuver performed by prey when they detect a threatening stimulus. Although its role in prey survival is not well studied, the neuromuscular control of the escape response has been extensively explored in animals as diverse as rodents, cephalopods, flies, and fishes (Eaton 1884). This research has revealed specialized circuits of neurons that activate muscles at high speed (Sillar et al. 2016), but with some directional control (Domenici et al. 2011a, Domenici et al. 2011b). Fishes employ the 'fast start' escape response, which is characterized by the body bending into a preparatory 'C' shape, followed by a rapid

acceleration generated by the body is it unfurls (Weihs 1973, Tytell and Lauder 2008). Although fish larvae do not exhibit the same degree of directional control shown in adults (Foreman and Eaton 1993), they are at least capable of directing a fast start toward either the left or right of the body (Stewart et al. 2014, Dunn et al. 2016). The role of escape responses in survival can be studied in the lab, where larvae may be subject to predation by adult zebrafish. The adults attempt to ingest larvae of their own species with suction feeding, which is typical of a broad diversity of fish predators (Wainwright et al. 2001, Stewart et al. 2013).

We performed experiments that replicated predator-prey interactions in zebrafish using a robotic predator. The robot allowed us to expose larvae to a controlled and repeatable stimulus (Stewart et al. 2014). It consisted of a dead and chemically fixed adult zebrafish that was suspended in the center of an aquarium populated with larvae. Through the action of a linear servomotor (Fig. 3.1A), the robot was translated through the aquarium at a constant speed (11 cm s^{-1}) that is similar to what is exhibited by a live zebrafish while foraging (Stewart et al. 2013). This motor also propelled two high-speed (250 frames s^{-1}) cameras that were mounted above the predator, where they recorded the responses of prey. Prey were generally motionless until exhibiting a fast start in response to the robot. From our video recordings, we measured the 3D position and orientation of each prey fish before and during their escape. Most prey escaped in a direction away from the robot (Fig. 3.1B) and at a distance > 2 cm outside the range of what may be stimulated by flow sensing and olfaction (Stewart et al. 2014). These responses were similar to those observed for zebrafish larvae in response to the projected image of an expanding disk (Dunn et al. 2016). Therefore, zebrafish larvae exhibited an escape response to our predator robot as a visual stimulus.
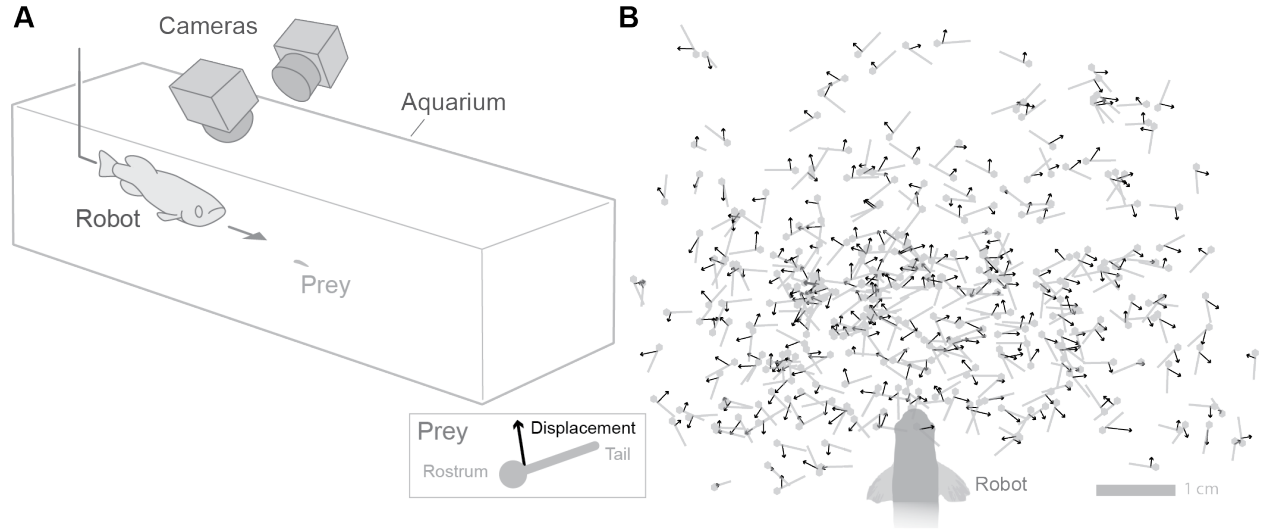
Fig. 3.1. Experimental measurements of the escape response stimulated by a predator robot. (A) The responses of prey were recorded with two high-speed video cameras that moved with the robot as it translated through a rectangular aquarium. (B) The 3D position (in gray) and direction (black arrow) of the escape response were measured from the video recordings.

We analyzed the directions of the visual stimulus and escape response from the perspective of each larva. These directions were calculated by transforming the 3D coordinates of the robot and the escape direction in the larva's frame of reference prior to the escape. This showed that the majority of responses were directed contralateral to the eye exposed to the predator robot (Fig. 3.2A). When the robot appeared in the left eye, the escape was directed toward the right more than three-quarters of the time ($P_{cont} = 0.80 \pm 0.05$, where P_{cont} is the probability of a contralateral response with ±95% confidence intervals, $n = 224$) and similar responses were elicited in the opposite direction ($P_{cont} = 0.73 \pm 0.06$, $n = 239$). Among contralateral responses, we did not find that the angle of an escape correlated with the stimulus angle of the robot (Linear Regression: $P = 0.75$, Fig. 3.2B). Instead, larvae escaped with a heading ($\theta = 106° \pm 10°$, $n = 502$) that was approximately normal to the initial orientation of the body irrespective of the stimulus direction, as previously observed (Stewart et al. 2014, Dunn et al. 2016).

We discovered that the probability of a contralateral response depends on the direction of a predator's approach. In particular, prey were more likely to respond with a contralateral response when the predator appeared in the central visual field ($P_{cont} = 0.87° \pm 0.04°$, for $30° \leq \lambda < 120°$, where λ is the angle of the predator in the visual field $n = 265$, Fig. 3.2C). Responses to the predator in peripheral vision were equally likely to elicit ipsilateral or contralateral responses either when the predator approached toward the rostral ($P_{cont} = 0.39 \pm 0.23$, for $-16° < \lambda < 20.6°$, $n = 18$) or caudal ($P_{cont} = 0.58 \pm 0.08$, for $130.4° < \lambda < 167°$, $n = 154$) ends of the body. This equal probability of the two possible directions demonstrates random and unpredictable behavior.

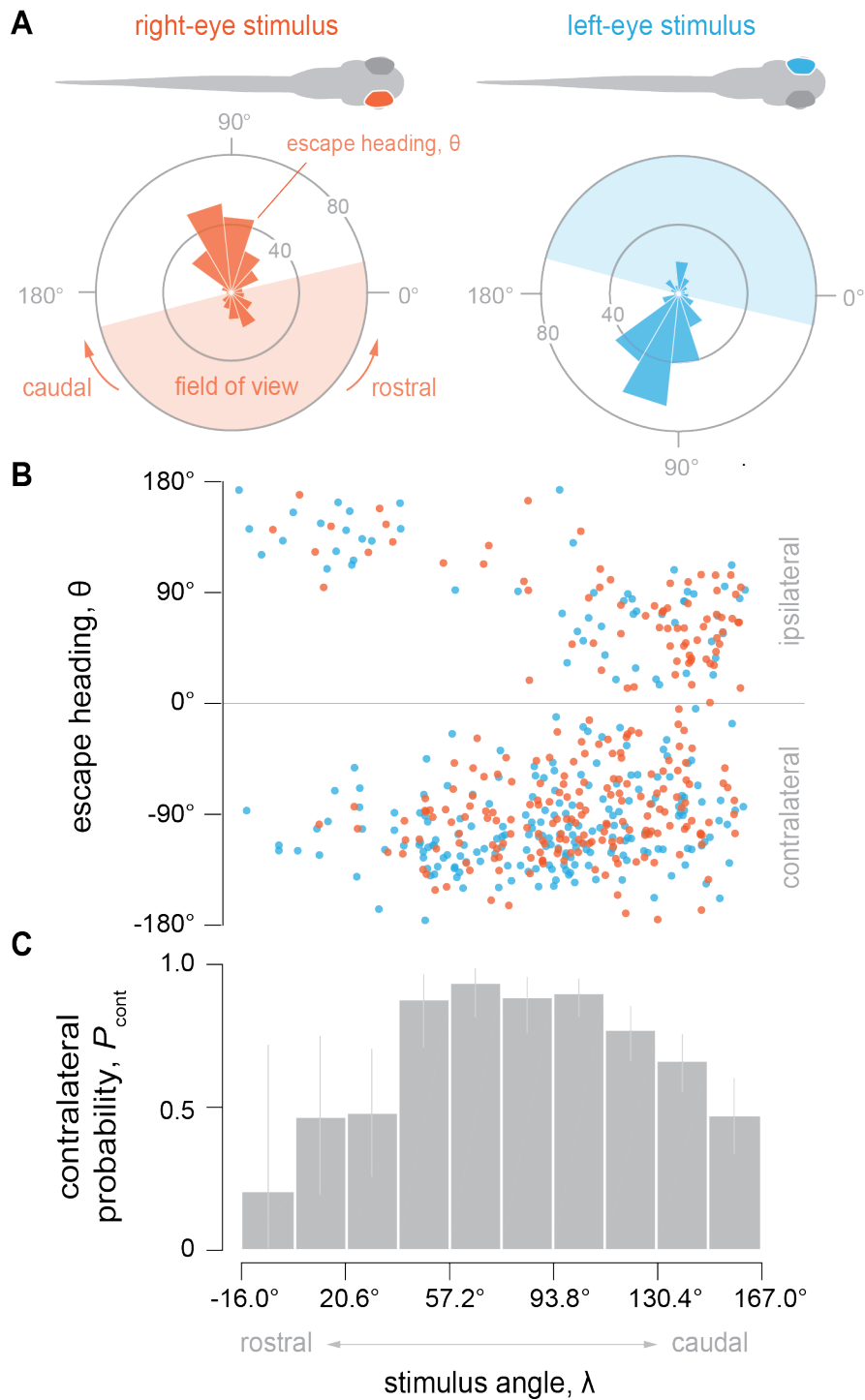**Fig. 3.2. The direction of the escape response relative to the visual stimulus.** (A) The frequency of the escape direction when the predator appeared on the left eye (in blue) and right eye (in red) of the prey. (B) The escape heading for the same responses as a function of the escape angle. (C) The probability of a contralateral response generated in equal intervals (18.3°) of the stimulus angle.

Therefore, zebrafish larvae employed a protean strategy, but only in response to a stimulus in the peripheral visual field. In contrast, responses to a central visual stimulus were consistently contralateral to the predator (Fig. 3.2C).

We developed a model to examine how our measurements of escape direction compare to the predictions of an optimal strategy. This model was based on previously developed pursuit-evasion theory (Weihs and Webb 1984, Soto et al. 2015), but incorporated the finding that the escape is restricted to a narrow range of angles (Fig. 3.2A) and is independent of the stimulus direction (Fig. 3.2B). We consequently modeled the escape direction as $90°$ from the initial body orientation (φ) and considered the implications of both contralateral and ipsilateral responses (Fig. 3.3A). Assuming a straight path for both animals, the distance between them was predicted and the minimum distance (d, normalized by the distance at which the escape is initiated) was determined from the speed of our robot and previous measurements for the escape response in larvae (Müller and van Leeuwen 2004). These calculations revealed that the minimum distance is maximized for contralateral responses (d_C) over a broad range of body orientations, but that body orientation has a strong effect on minimum distance (d_I) in ipsilateral responses (Fig. 3.3C). The difference between these predictions ($d_C - d_I$) indicates the strategic advantage to a contralateral response over the alternative.

The contralateral advantage varies with body orientation in a relationship that approximates a negative quadratic (Fig. 3.3C). This relationship indicates that prey have the greatest strategic benefit to a contralateral response when the predator approaches at a right angle with respect to the body ($\varphi = 90°$). Such an approach would appear in the central visual field of a larva, which we found consistently elicits a contralateral response (Fig. 3.2C).
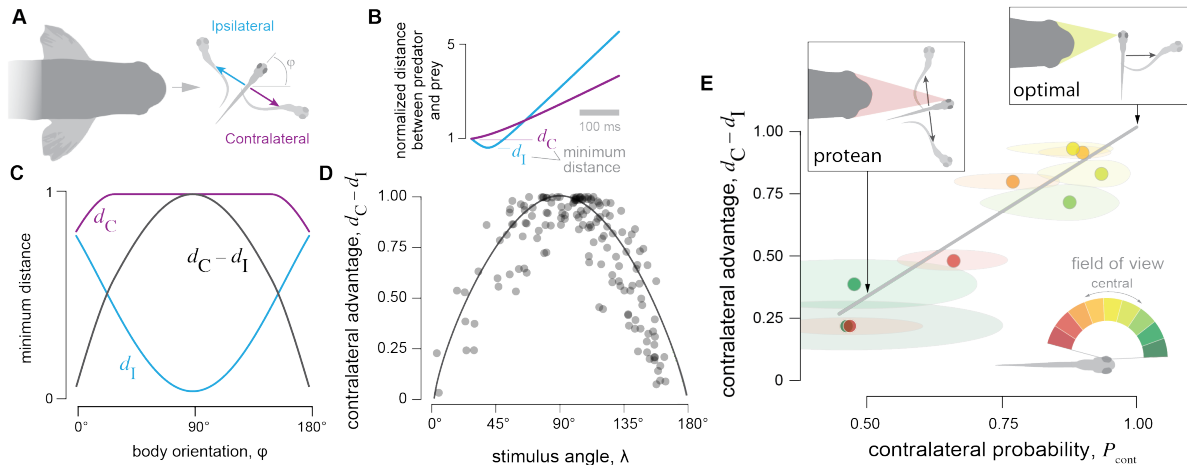
Fig. 3.3. The strategic implications of escape heading. (A) We modeled the escape response as occurring at a right angle from the initial orientation of the body (φ) for contralateral (purple) and ipsilateral (blue) escape responses for prey aligned with the heading of the predator. (B) For each response, the distance between predator and prey may be predicted, assuming a constant heading and speed. The minimum distance was calculated for contralateral (d_C) and ipsilateral (d_I) escapes and (C) this was determined for all body orientations. The difference in minimum distance between ipsilateral and contralateral responses (black curve, $d_C - d_I$) represents the contralateral advantage. We calculated the contralateral advantage (gray circles) for all positions and orientations recorded in our experiments (Fig. 3.1B). (D) The contralateral probability (values from Fig. 3.2C) is positively correlated with the contralateral advantage, when binned with respect to the visual field ($r^2 = 0.66$, $P < 0.001$, $n = 10$). A contralateral advantage of unity represents an optimal advantage to an escape in that direction. At the opposite end of this relationship, a protean strategy is indicated by an equal probability of ipsilateral and contralateral responses ($P_{cont} = 0.50$).

In contrast, there is little contralateral advantage at orientations when the prey is directed toward ($\varphi \sim 180°$) or away ($\varphi \sim 0°$) from the predator. Under these circumstances, the predator appears in the peripheral vision of the prey, which we found to elicit an equal probability between contralateral and ipsilateral responses (Fig. 3.2C).

A comparison between the predictions of our mathematical model and our measurements of escape direction reveals a compelling relationship. We found a strong positive correlation between our observed probability of a contralateral response and the contralateral advantage (linear regression: $r^2 = 0.66$, $P < 0.001$, $n = 10$). This indicates that prey respond with a protean strategy ($P_{cont} = 0.5$) when there exists little strategic benefit to a contralateral escape. If the predator instead approaches at an angle closer to a right angle with respect to the prey's orientation, the advantage to a contralateral responses increases (Fig. 3.3C) and we found responses toward that side to occur with greater frequency (Fig. 3.2C). Therefore, zebrafish larvae exhibit a continuum in strategy between protean ($P_{cont} = 0.5$) and optimal ($d_C - d_I = 1$) extremes.

This continuum strategy informs our understanding for the neurophysiology of the escape response in zebrafish larvae. A looming stimulus is detected in a fish brain by a region known as the optic tectum (Dunn et al. 2016), which is structured with a topographic map of the retinal cells that span the visual field (Stuermer 1988, Nikolaou et al. 2012). Therefore, a predator approaching the side of a prey's body will stimulate the central region of the retina and active a region of the brain that is distinct from a peripheral stimulus. Each of these regions is capable of activating the motor program for an escape (Dunn et al. 2016, Zotolli et al. 1987). Escapes activated by the optic tectum are controlled by left and right sets of neurons in the hindbrain, known as the Mauthner neuron and its serial homologs (Dunn et al. 2016). The premotor

interneurons that activate these regions are capable of inhibiting one side of the body while activating the other and thereby creating a competition that determines the side of the body that activates the escape (Koyama et al. 2016). Our results suggest that the region of the optic tectum that is activated by a central stimulus strongly biases the outcome of this competition in favor of the contralateral side. The brain regions activated by a peripheral stimulus offer no such favoritism and consequently exhibit an equal probability between contralateral and ipsilateral responses.

The continuum strategy is likely not unique to larval fish. Similar kinematics have been observed in shrimp (Arnott et al. 1999) and crabs (Woodbury 1986), which also escape laterally with a limited range in heading. The continuum strategy may therefore offer a common means for prey to combine the benefits of optimal (Weihs and Webb 1984) and protean (Humphries and Driver 1970) strategies. This contrasts the classic literature, which presents these strategies as a mutually exclusive dichotomy. The continuum strategy therefore articulates a new paradigm for prey survival that may have broad implications for the evolution and ecology of escape responses.

Methods supplement

Animal Husbandry

Our experiments considered how larval zebrafish (*Danio rerio*, Hamilton 1822) evade predators. All zebrafish were bred from wild-type (AB line) colonies housed in a flow-through tank system (Aquatic Habitats, Apopka, FL, USA) that was maintained at 28.5 °C on a 14 h:10 h light:dark cycle. The fertilized eggs from randomized mating were cultured according to standard techniques (Westerfield, 1993). All larvae were 5 days post-fertilization, with a total number of 705 larvae used in all experiments. The experimental methods were approved by the Institutional Animal Care and Use Committee of the University of California, Irvine (protocol 2004-2554).

Robotic Predator Experiments

A robot allowed us to replicate a predator's approach toward prey with controlled and repeatable motion (Fig. 3.1). The body of a formalin-fixed dead adult zebrafish served as the predator mimic, which was translated through the center of a water-filled tank (length x height x width = 36 cm x 8 cm x 9 cm, water temperature: 27 °C) that contained between 100 and 200 larvae. The predator was affixed to a sting that was anchored to a sled that ran along a rail system (high-speed 23 mm needle-roller carriages on 64 mm guide rails, McMaster-Carr, Santa Fe Springs, CA, USA). The sled was driven by a magnetic-drive linear servomotor (model P01-23160, LinMot Inc., Elkhorn, WI, USA) at a constant speed (11 cm s^{-1}). This speed approximated the average that was previously measured in adult zebrafish during foraging (Stewart et al. 2013). The sled additionally carried two high-speed video cameras (Photon Focus DR1, Norpix Inc., Montreal, CA, 500 frames s^{-1} at 640 x 480 pixel) positioned above the robot, which focused on the predator's head and region anterior to the predator (8.00 cm x 6.00 cm) from two oblique perspectives (Fig. 3.1A). Prior to an experiment, larvae were acclimated to the aquarium for 20

min, during which the robot was concealed from view with a partition. At the start of an experiment, the partition was lifted and the robot was translated through the water, where it encountered most larvae at a position between the middle and far end of the aquarium. To minimize repeated measures from the same larva, we ceased experiments on groups of larvae once the number of recorded escape responses exceeded 15% of the total number of prey within the chamber.

Data Acquisition and Analysis

We performed a kinematic analysis to determine how visual cues affect the direction of the escape response in prey. In particular, we measured the 3D location of each larva before and after initiating a 'fast-start' escape response (Kimmel et al. 1974). This was achieved with custom software developed in Matlab (v.2014b, with the Image Processing Toolbox, MathWorks, Natick, MA, USA) to digitize three landmarks along the prey body from the video recording of both cameras. These landmarks consisted of the anterior margin of the rostrum and the posterior margins of the swim bladder and tail. The body's center of mass was estimated as the posterior margin of the swim bladder, which is consistent with prior measurements (Stewart et al. 2010). A fast start was identified by when a larva body rapidly (< 15 ms) curled into a 'C'-shape, which is characteristic of first stage of this behavior (Kimmel et al. 1974, Weihs 1973). We obtained body coordinates for the video frame prior to motion, the 'initial position', as well as when the body fully unfurled from the 'C' shape, which corresponds to the completion of the fast start. This event was identified by a reversal in motion by the head of the larva from direction of yawing. In the present investigation and past work (Stewart et al. 2014, Nair et al. 2015), we found that the heading at this time approximates the direction of the undulatory swimming that follows during an escape. To avoid analyzing the responses of larvae that might

72

have responded to conspecifics, we excluded a larva if it was positioned within 5 body lengths of another responding larva.

We analyzed the landmarks from our video recordings to resolve the 3D kinematics of the escape response. The calibration for this analysis used a static body that was constructed with 27 landmarks of known relative 3D position. These landmarks were visible from both cameras when it was placed in the center of the tank. A direct-linear transform was calculated using 'Digitizing Tools' software in MATLAB (2015a, MathWorks, Natick, MA, USA) (Hedrick 2008) from manually selected coordinates of the landmarks from the two camera perspectives. Using a custom script in MATLAB, we found the body points of the zebrafish larvae and the rostrum of the robotic predator by selecting landmarks from the two camera views and using the direct-linear transform to find their coordinates in 3D space. These coordinates allowed us to define the initial position and heading of a prey in the predator's frame of reference. The predator's frame of reference was defined with its origin at the anterior margin of the predator's rostrum. The x-axis of this system was found by the velocity of the origin and the z-axis as the direction opposing gravity. We found the direction of gravity by recording two coordinates along a nylon wire that was suspended between a buoyant sphere at the surface of the water and weight submerged beneath the surface. Following the convention for a right-handed coordinate system, the y-axis was consequently defined as the lateral left direction of the predator's body. A prey's heading, θ, was determined by the displacement of the center of mass from the initial position to the completion of the fast start. Although the heading was described in 3D, responses were generally planar and we therefore characterized its direction by the azimuth angle in the predator's coordinate system.

The direction of the approaching predator was measured to relate the fast start to visual stimuli. The stimulus angle was defined as the position of the predator in the prey's frame of reference. For each larva based on the their angular position, ψ, and orientation, ϕ, in the predator's frame of reference. ψ was its angular deviation created between its position in space away from the predator's path. ϕ was the angular deviation of the larva's anteroposterior axis away from the predator's path (Fig. 3.3A). To calculate the stimulus angle, the following equation was used:

$$\lambda = \pi - |\psi| + \phi \frac{\psi}{|\psi|} \qquad (3.1)$$

We defined the field of view for each eye as the sum of the anatomical range of the retina (167°) (Easter and Nicola 1996) and its rotation (20°) (Patterson et al. 2013). This field of view is rotated toward the anterior of the body by -16°.

Larval zebrafish performed a contralateral or an ipsilateral response when escaping from the robotic predator. To determine whether a larva committed to a contralateral or ipsilateral response, the stimulus angle of each larva was compared to its escape heading. If the larva's stimulus angle was in the same lateral hemisphere (left or right) as the escape heading, then the larva was considered to have performed an ipsilateral response. Otherwise, the larva was considered to do a contralateral response.

We measured the probability of observing a contralateral response as it varied with stimulus angle. To calculate the probability of a contralateral response, all responses were divided into 10 equal intervals over the field of view. Within each interval, the contralateral probability was calculated as the ratio of contralateral responses to the total number of responses (Fig. 3.2C). A 95% confidence interval for each bin was calculated assuming a binomial distribution (Johnson et al. 1993).

74

Mathematical Modeling

We used a differential game theory model to evaluate the effectiveness of larval escape responses (Isaacs 1965, Weihs and Webb 1984). In this model, a pursuer (the robotic predator) approached an evader (the larval zebrafish) along a straight path, starting at an initial distance, R0. With this model, we calculated the minimum distance, *d*, between the pursuer and evader, given the escape of the evader. The minimum distance was the shortest, two-dimensional distance between the pursuer and evader as the pursuer moves along the straight path and the evader escapes with a fixed angle, α, away from this path. The minimum distance was normalized by R_0, meaning the minimum distance could only range between 0 and 1. Minimum distance was a key parameter for prey survival since the closer a prey was to its predator, the more likely it would be captured (Weihs et al. 1984). Therefore, greater minimum distances conveyed a more effective escape by the evader. To calculate minimum distance, we used a modified model (Soto et al. 2015):

$$d(\alpha, \psi) = \frac{(\sin(\alpha - \psi) + K\sin(\psi))^2}{K^2 + 2K\cos(\alpha) + 1}, K \geq \cos(\alpha) \qquad (3.2)$$

$$d(\alpha, \psi) = 1, K < \cos(\alpha), \qquad (3.3)$$

where and were the escape heading and the angular position, relative to the approach of the predator respectively. *K* was the ratio of predator speed to prey speed. To calculate the contralateral advantage for each larva, we assumed the prey would escape with a contralateral or ipsilateral response, using a 90° turn. We calculated the minimum distance for contralateral and ipsilateral responses, assuming α equaled the orientation of the larva $\pm 90^\circ$. The contralateral advantage was calculated as the difference in minimum distance between a contralateral response and an ipsilateral response. The 95% confidence interval for the contralateral advantage (Fig. 3.4) was calculated assuming a normal distribution (Patel and Read 1993).

REFERENCES

Akerboom, J., Chen, T., Wardill, T., Tian, L., Marvin, J., Mutlu, S., Calderon, N., Esposti, F., Borghuis, B., Sun, X. et al. (2012). Optimization of a GCaMP calcium indicator for neural activity imaging. *J. Neurosci.* **32**, 13819-13840.

Arnott, S., Neil, D. and Ansell, A. (1999). Escape trajectories of the brown shrimp *Crangon crangon*, and a theoretical consideration of initial escape angles from predators. *J. Exp. Biol.* **202**, 193—209.

Bagnall, M. and McLean, D. (2014). Modular organization of axial microcircuits in Zzebrafish. *Science* **343**, 197–200.

Barbosa, P. and Castellanos, I., eds (2005). *Ecology of Predator-Prey Interactions.* Oxford, United Kingdom: Oxford University Press.

Barlow, G. (1968). Modal action patterns. In *How Animals Communicate* (ed. T. Seboek), pp. 261-268. Bloomington, IN: University Press.

Bianco, I., Kampff, A. and Engert, F. (2011). Prey capture behavior evoked by simple visual stimuli in larval zebrafish. *Front. Syst. Neurosci.* **5**, 101.

Bianco, I. and Engert, F. (2015). Visuomotor transformations underlying hunting behavior in zebrafish. *Curr. Biol.* **25**, 831–846.

Broom, M. and Ruxton, G. (2005). You can run—or you can hide: optimal strategies for cryptic prey against pursuit predators. *Behav. Ecol.* **16**, 534–540.

Bullock, T. (1984). Comparative Neuroethology of Startle, Rapid Escape, and Giant Fiber-Mediated Responses. In *Neural Mechanisms of Startle Behavior* (ed. R. Eaton), pp. 1–13. Boston, MA: Springer.

Burgess, H. and Granato, M. (2007). Modulation of locomotor activity in larval zebrafish during light adaptation. *J. Exp. Biol.* **210**, 2526-2539.

Catania K. (2009). Tentacled snakes turn C-starts to their advantage and predict future prey behavior. *Proc. Nat. Acad. Sci.* **106**, 11183–11187.

Combes, S., Rundle, D., Iwasaki, J. and Crall, J. (2012). Linking biomechanics and ecology through predator–prey interactions: flight performance of dragonflies and their prey. *J. Exp. Biol* **215**, 903–913.

Cooper, W. and Blumstein, D., ed. (2015). *Escaping From Predators.* Cambridge, United Kingdom: Cambridge Univ. Press.

Corcoran, A. and Conner, W. (2016). How moths escape bats: predicting outcomes of predator-prey interactions. *J. Exp. Biol.* **219**, 2704–2715.

Craig, J., ed. (1989). *Introduction To Robotics: Mechanics and Control.* New York: Addison-Wesley.

Curio, E. (2012). *The Ethology of Predation.* New York, NY: Springer.

Dill, L. (1974). The escape response of the zebra danio (*Brachydanio rerio*), I. The stimulus for escape. *Anim. Behav* **22**, 711-722.

Domenici, P. and Blake, R. (1997). The kinematics and performance of fish fast-start swimming. *J. Exp. Biol.* **200**, 1165-1178.

Domenici, P. (2001). The scaling of locomotor performance in predator–prey encounters: from fish to killer whales. *Comparative Biochem. and Phys. Part A* **131**, 169–182.

Domenici, P., Blagburn, J. and Bacon, J. (2011a). Animal escapology I: theoretical issues and emerging trends in escape trajectories. *J. Exp. Biol.* **214**, 2463–2473.

Domenici, P., Blagburn, J. and Bacon, J. (2011b). Animal escapology II: escape trajectory case studies. *J. Exp. Biol.* **214**, 2474–2494.

Dunn, T., Gebhardt, C., Naumann, E., Riegler, C., Ahrens, M., Engert, F. and Del Bene, F. (2016). Neural Circuits Underlying Visually Evoked Escapes in Larval Zebrafish. *Neuron* **89**, 613–628.

Easter, S. and Nicola G. (1996). The Development of Vision in the Zebrafish (*Danio rerio*). *Dev. Biol.* **180**, 646-663.

Eaton, R. and Farley, R. (1975). Mauthner neuron field potential in newly hatched larvae of zebrafish. *J. Neurophysiol.* **38**, 502–512.

Eaton, R., Lavender, W. and Wieland, C. (1981). Identification of Mauthner-initiated response patterns in goldfish: Evidence from simultaneous cinematography and electrophysiology. *J. Comp. Phys.* **144**, 521-531.

Eaton, R., ed. (1984). *Neural Mechanisms of Startle Behavior.* New York, NY: Springer.

Eaton, R., DiDomenico, R. and Nissanov, J. (1988). Flexible body dynamics of the goldfish C-start: implications for reticulospinal command mechanisms. *J. Neurosci.* **8**, 2758–2768.

Eaton, R., DiDomenico, R. and Nissanov, J. (1991). Role of the Mauthner Cell in Sensorimotor Integration by the Brain Stem Escape Network. *Brain Behav. Evol.* **37**, 272–285.

Eaton, R. and Emberley, D. (1991). How stimulus direction determines the trajectory of the Mauthner-initiated escape response in a teleost fish. *J. Exp. Biol.* **161**, 469-487.

Fernald R. (1988). Aquatic adaptations in fish eyes. In *Sensory Biology of Aquatic Animals* (eds. Atema, J., Fay, R., Popper, A., and Tavolga, W.), pp. 435-466. New York: Springer-Verlag.

Ferry-Graham, L., Wainwright, P. and Lauder, G. (2003). Quantification of flow during suction feeding in bluegill sunfish. *Zoology* **106**, 159–168.

Fetcho, J., Higashijima, S. and McLean, D. (2008). Zebrafish and motor control over the last decade. *Brain Res. Rev.* **57**, 86-93.

Foreman, M. and Eaton, R. C. (1993). The direction change concept for reticulospinal control of goldfish escape. *J. Neurosci.* **13**, 4101–4113.

Fuiman, L. (1994). The interplay of ontogeny and scaling in the interactions of fish larvae and their predators. *J. Fish. Biol.* **45**, 55–79.

Gabbiani, F., Krapp, H. and Laurent, G. (1999). Computation of object approach by a wide-field, motion-sensitive neuron. *J. Neurosci.* **19**, 1122–1141.

Ghose, K., Horiuchi, T., Krishnaprasad, P. and Moss, C. (2006). Echolocating bats use a nearly time-optimal strategy to intercept prey. *PLoS biology* **4**, e108.

Hamilton, F. (1822). *An Account of the Fishes Found in the River Ganges and its Branches*. Archibald Constable and Company, Edinburgh.

Hedrick, T. (2008). Software techniques for two and three-dimensional kinematic measurements of biological and biomimetic systems. *Bioinspir. Biomim.* **3**, 034001.

Heuch, P., Doall, M. and Yen, J. (2007). Water flow around a fish mimic attracts a parasitic and deters a planktonic copepod. *J.Plank. Res.* **29**, i3–i16.

Higham, T. (2005). Sucking while swimming: evaluating the effects of ram speed on suction generation in bluegill sunfish, *Lepomis macrochirus*, using digital particle image velocimetry. *J. Exp. Biol.* **208**, 2653–2660.

Higham, T. (2007). Feeding, fins and braking maneuvers: locomotion during prey capture in centrarchid fishes. *J. Exp. Biol.* **210**, 107-117.

Higham, T. E.,Hulsey, C. D., Rícan, O. and Carroll, A. (2007). Feeding with speed: prey capture evolution in cichilds. *J. Evol. Biol.* **20**, 70–78.

Holzman, R., Day, S. and Wainwright, P. (2007). Timing is everything: coordination of strike kinematics affects the force exerted by suction feeding fish on attached prey. *J Exp. Biol.* **210**, 3328–3336.

Holzman, R., Collar, D., Day, S., Bishop, K. and Wainwright, P. (2008). Scaling of suction-induced flows in bluegill: morphological and kinematic predictors for the ontogeny of feeding performance. *J. Exp. Biol.* **211**, 2658–2668.

Holzman, R. and Wainwright, P. (2009). How to surprise a copepod: Strike kinematics reduce hydrodynamic disturbance and increase stealth of suction-feeding fish. *Limnol. Oceanogr.* **54**, 2201–2212.

Howland, H. (1974). Optimal strategies for predator avoidance: The relative importance of speed and maneuverability. *J. Theor. Biol.* **47**, 333–350.

Huang, K. H., Ahrens, M. B., Dunn, T. and Engert, F. (2013). Spinal projection neurons control turning behaviors in zebrafish. *Curr. Biol*. **23**, 1566-1573.

Humphries, D. A. and Driver, P. M. (1970). Protean defence by prey animals. *Oecologia* **5**, 285–302.

Isaacs R. (1965). *Differential games: a mathematical theory with applications to warfare and pursuit, control and optimization.* New York, NY: John Wiley and Sons, Inc.

Johnson, G. (1926). Studies on the functions of the giant nerve fibers of crustaceans, with special reference to Cambarus and Palaemonetes. *J. Comp. Neurol.* **42**, 19–33.

Johnson, S. (2012). *The Optics of Life: A Biologist's Guide to Light in Nature*. Princeton, NY: Princeton University Press.

Johnson, N., Kemp, A. and Kotz, S. (1993). *Univariate Discrete Distributions*. New York, NY: John Wiley & Sons, Inc.

Kimmel C., Patterson J. and Kimmel R. (1972). The Development and Behavioral Characteristics of the Startle Response in the Zebra Fish. *Dev. Psychobiol.* **24**, 47-60.

Kimmel, C., Eaton, R. and Powell, S. (1980). Decreased fast-start performance of zebrafish larvae lacking Mauthner neurons. *J. Comp. Physiol. A* **140**, 343-350.

Korn H. and Faber D. (2008). The Mauthner Cell Half a Century Later: Review A Neurobiological Model for Decision-Making? Neuron, **47**, 13-28.

Koyama, M., Minale, F., Shum, J., Nishimura, N., Schaffer, C., Fetcho, J. and Calabrese, R. (2016). A circuit motif in the zebrafish hindbrain for a two alternative behavioral choice to turn left or right. *eLife Sciences* **5**, e16808.

Li, G., Müller, U., van Leeuwen, J. and Liu, H. (2016). Fish larvae exploit edge vortices along their dorsal and ventral fin folds to propel themselves. *J. R. Soc. Interface* **13**, 20160068.

Liu, K. S. and Fetcho, J. R. (1999). Laser ablations reveal functional relationships of segmental hindbrain neurons in zebrafish. *Neuron* **23**, 325–335.

Massey, F. (1951). The Kolmogorov-Smirnov Test for Goodness of Fit. *J. Am. Stat. Assoc.* **46**, 68–78.

McHenry, M. and Lauder, G. (2005). The mechanical scaling of coasting in zebrafish (*Danio rerio*). *J. Exp. Biol.* **208**, 2289–2301.

McHenry, M. and Liao, J. (2014). The Hydrodynamics of Flow Sensing. In *Springer Handbook of Auditory Research*, 48: The Lateral Line. New York: Springer.

Menelaou, E. and McLean, D. (2012). A gradient in endogenous rhythmicity and oscillatory drive matches recruitment order in an axial motor pool. *J. Neurosci.* **32**, 10925-10939.

Moyes, C. and Schulte, P. (2006). *Principles of Animal Physiology*. San Francisco, CA: Peerson Benjamin Cummings.

Müller, U. and van Leeuwen, J. (2004). Swimming of larval zebrafish: ontogeny of body waves and implications for locomotory development. *J. Exp. Biol.* **207**, 853–868.

Nair, A., Azatian, G. and McHenry, M. (2015). The kinematics of directional control in the fast start of zebrafish larvae. *J. Exp. Biol.* **218**, 3996–4004.

Nakayama, H. and Oda, Y. (2004). Common sensory inputs and differential excitability of segmentally homologous reticulospinal neurons in the hindbrain. *J. Neurosci.* **24**, 3199-3209.

Nikolaou, N., Lowe, A., Walker, A., Abbas, F., Hunter, P., Thompson, I. and Meyer, M. (2012). Parametric functional maps of visual inputs to the tectum. *Neuron* **76**, 317-324.

Nissanov, J., Eaton, R. and DiDomenico, R. (1990). The motor output of the Mauthner cell, a reticulospinal command neuron. *Brain Res*. **517**, 88-98.

O'Malley, D., Kao, Y. and Fetcho, J. (1996). Imaging the functional organization of zebrafish hindbrain segments during escape behaviors. *Neuron* **17**, 1145–1155.

Patel, J. and Read, C. (1996). *Statistics: A Series of Textbooks and Monographs*. Boca Raton, FL: CRC Press.

Patterson B., Abraham, O., MacIver, M. and McLean, D. (2013). Visually guided gradation of prey capture movements in larval zebrafish. *J. Exp. Biol.* **216**, 3071-3083.

Peterson, B. (1984). The reticulospinal system and its role in the control of movement. In *Brain Stem Control of Spinal Cord Function* (ed. C. D. Barnes), pp. 27-86. New York, NY: Academic.

Pitcher, J. (1986). Functions of shoaling behaviour in teleosts. In *The Behaviour of Teleost Fishes* (ed. J. Pitcher), chapter 12, pp. 294–337. Springer.

Shifferman, E. and David, J. (2004). Movement and direction of movement of a simulated prey affect the success rate in barn owl Tyto alba attack. *J. Avian. Biol.* **35**, 111–116.

Sillar, K., Picton, L. and Heitler, W. (2016). *The Neuroethology of Predation and Escape, vol. 1*. Hoboken, NJ: Wiley-Blackwell.

Stewart, W. and McHenry, M. (2010). Sensing the strike of a predator fish depends on the specific gravity of a prey fish. *J. Exp. Biol.* **213**, 3769-3777.

Stewart, W., Cardenas, G. and McHenry, M. (2013). Zebrafish larvae evade predators by sensing water flow. *J. Exp. Biol.* **216**, 388–398.

Stewart, W., Nair, A., Jiang, H. and McHenry, M. (2014). Prey fish escape by sensing the bow wave of a predator. *J. Exp. Biol.* **217**, 4328–4336.

Stuermer, C. (1988). Retinotopic organization of the developing retinotectal projection in the zebrafish embryo. *J. Neurosci.* **8**, 4513-4530.

Soto, A., Stewart, W. and McHenry, M. (2015). When Optimal Strategy Matters to Prey Fish. *Integr. Comp. Biol.* **55**, 110–120.

Robinson, J., Schmitt, E., Hárosi, F., Reece, R. and Dowling, J. (1993). Zebrafish ultraviolet visual pigment: absorption spectrum, sequence, and localization. *Proc. Natl. Acad. Sci.* **90**, 6009–6012.

Temizer, I., Donovan, J., Baier, H. and Semmelhack, J. (2015). A Visual Pathway for Looming-Evoked Escape in Larval Zebrafish. *Current Biology*, **25**, 1823-1834.

Terborgh, J. and Estes, D., eds (2010). *Trophic Cascades: Predators, Prey, and the Changing Dynamics of Nature.* Washington, DC, USA: Island Press.

Tinbergen, N. (1951). *The study of instinct.* Oxford, United Kingdom: Oxford University Press.

Tytell, E. and Lauder, G. (2008). Hydrodynamics of the escape response in bluegill sunfish, *Lepomis macrochirus*. *J. Exp. Biol.* **211**, 3359-3369

Wainwright, P., Ferry-Graham, L., Waltzek, T., Carroll, A., Hulsey, C. and Grubich, J. (2001). Evaluating the use of ram and suction during prey capture by cichlid fishes. *J. Exp. Biol.* **204**, 3039–3051.

Waldman, B. (1982). Quantitative and developmental analyses of the alarm reaction in the zebra danio, *Brachydanio rerio*. *Copeia* **1982**, 1–9.

Walker, J., Ghalambor, C., Griset, O., McKenney, D. and Reznick, D. (2005). Do faster starts increase the probability of evading predators? *Func. Ecol.* **19**, 808–815.

Webb, P. (1982). Avoidance responses of fathead minnow to strikes by four teleost predators. *J. Comp. Phys.* **96**, 93-106.

Webb, P. (1984). Body and fin form and strike tactics of four teleost predators attacking fathead minnow (*Pimephales promelas*) prey. *Can. J. Fish Aquat. Sci.* **41**, 157–165.

Weihs D. (1973). The mechanism of rapid starting of slender fish. *Biorheo.* **10**, 343-350.

Weihs, D. and Webb, P. (1984). Optimal avoidance and evasion tactics in predator-prey interactions. *J. Theo. Biol.* **106**, 189–206.

Westerfield, M., McMurray, J. and Eisen, J. (1986). Identified motoneurons and their innervation of axial muscles in the zebrafish. *J. Neurosci.* **6**, 2267-2277.

Westerfield, M. (1993). *The Zebrafish Book: A Guide for the Laboratory Use of Zebrafish (Brachydanio rerio)*. Eugene, OR: University of Oregon Press.

Woodbury, P. (1986). The geometry of predator avoidance by the blue crab, *Callinectes sapidus Rathbun*. *Anim. Behav.* **34**, 28-37.

Ydenberg, R. and Dill, L. (1986). The economics of fleeing from predators. *Adv. Stud. Behav.* **16**, 229–249.

Young, J. (1938). The Functioning of the Giant Nerve Fibres of the Squid. *J. Exp. Biol.*, **15**, 170–185.

Zottoli, S., Hordes, A. and Faber, D. (1987). Localization of optic tectal input to the ventral dendrite of the goldfish Mauthner cell. *Brain*